frontiers in
SYSTEMS NEUROSCIENCE

ORIGINAL RESEARCH ARTICLE
published: 28 November 2011
doi: 10.3389/fnsys.2011.00089

Reduced pallidal output causes dystonia

Atsushi Nambu[1]*, Satomi Chiken[1], Pullanipally Shashidharan[2], Hiroki Nishibayashi[3], Mitsuhiro Ogura[3], Koji Kakishita[3], Satoshi Tanaka[3], Yoshihisa Tachibana[1], Hitoshi Kita[4] and Toru Itakura[3]

[1] *Division of System Neurophysiology, National Institute for Physiological Sciences and Department of Physiological Sciences, Graduate University for Advanced Studies, Okazaki, Japan*
[2] *Department of Neurology, Mount Sinai School of Medicine, New York, NY, USA*
[3] *Department of Neurological Surgery, Wakayama Medical University, Wakayama, Japan*
[4] *Department of Anatomy and Neurobiology, College of Medicine, University of Tennessee Health Science Center, Memphis, TN, USA*

Edited by:
Charles J. Wilson, University of Texas at San Antonio, USA

Reviewed by:
Thomas Wichmann, Emory University, USA
Jose Obeso, Universidad de Navarra, Spain

***Correspondence:**
Atsushi Nambu, Division of System Neurophysiology, National Institute for Physiological Sciences, 38 Nishigonaka, Myodaiji, Okazaki 444-8585, Japan.
e-mail: nambu@nips.ac.jp

Dystonia is a neurological disorder characterized by sustained or repetitive involuntary muscle contractions and abnormal postures. In the present article, we will introduce our recent electrophysiological studies in hyperkinetic transgenic mice generated as a model of DYT1 dystonia and in a human cervical dystonia patient, and discuss the pathophysiology of dystonia on the basis of these electrophysiological findings. Recording of neuronal activity in the awake state of DYT1 dystonia model mice revealed reduced spontaneous activity with bursts and pauses in both internal (GPi) and external (GPe) segments of the globus pallidus. Electrical stimulation of the primary motor cortex evoked responses composed of excitation and subsequent long-lasting inhibition, the latter of which was never observed in normal mice. In addition, somatotopic arrangements were disorganized in the GPi and GPe of dystonia model mice. In a human cervical dystonia patient, electrical stimulation of the primary motor cortex evoked similar long-lasting inhibition in the GPi and GPe. Thus, reduced GPi output may cause increased thalamic and cortical activity, resulting in the involuntary movements observed in dystonia.

Keywords: dystonia, globus pallidus, extracellular recording, stereotactic surgery, movement disorders

INTRODUCTION

Dystonia is a neurological disorder characterized by sustained or repetitive involuntary muscle contractions and abnormal postures. The pathophysiology of dystonia is poorly understood. No consistent neuropathological or biochemical changes have been detected yet. On the other hand, abnormal neuronal activity in the basal ganglia has been reported during stereotactic surgery for deep brain stimulation (DBS) in dystonia patients (Vitek et al., 1999; Zhuang et al., 2004; Starr et al., 2005; Tang et al., 2007).

In the present article, we will introduce our recent electrophysiological studies in hyperkinetic transgenic mice generated as a model of DYT1 dystonia (Chiken et al., 2008) and in a human cervical dystonia patient (Nishibayashi et al., 2011), and discuss the pathophysiology of dystonia on the basis of these electrophysiological findings. Firstly, we investigated the neuronal activity in the entopeduncular nucleus and globus pallidus in transgenic model mice of DYT1 dystonia (Chiken et al., 2008), the most common type of human primary generalized dystonia. Secondly, we also had a chance to record neuronal activity in the internal (GPi) and external (GPe) segments of the globus pallidus of a human cervical dystonia patient during stereotactic surgery (Nishibayashi et al., 2011). The entopeduncular nucleus and globus pallidus in rodents correspond to the GPi and GPe in primates, respectively, and thus, we will call these nuclei GPi and GPe hereafter. The GPi and GPe are two important nuclei in the basal ganglia circuitry, and their abnormal neuronal activity has been reported in movement disorders. We paid special attention to the responses of GPi and GPe neurons evoked by cortical stimulation. In voluntary movements, activity originating in the cortex is transmitted through the basal ganglia circuitry and finally reaches the output station of the basal ganglia, i.e., the GPi. Cortical stimulation can mimic information processing through the basal ganglia circuitry (Nambu et al., 2002; Tachibana et al., 2008). Motor cortical stimulation typically induces triphasic responses composed of early excitation, inhibition, and late excitation in GPi and GPe neurons of normal monkeys and rodents (Yoshida et al., 1993; Nambu et al., 2000; Chiken and Tokuno, 2003). The origin of each component has been identified, with the amplitudes and durations reflecting neuronal activity of the corresponding basal ganglia pathways and nuclei. In the studies by Chiken et al. (2008) and Nishibayashi et al. (2011), long-lasting inhibition was evoked in the GPi and GPe of both DYT1 dystonia model mice and a human cervical dystonia patient.

MATERIALS AND METHODS

ANIMAL STUDY

The DYT1 gene on chromosome 9q34 codes the torsinA protein (Ozelius et al., 1997). A three-base pair (GAG) deletion in the DYT1 gene, resulting in the loss of a glutamic acid residue (ΔE) in the torsinA protein (Ozelius et al., 1997), causes human DYT1 dystonia. Recently, Shashidharan et al. (2005) generated a transgenic mouse model by overexpression of human ΔE-torsinA. These transgenic mice developed hyperkinesia and rapid bidirectional circling. They also exhibited abnormal involuntary movements with dystonic-appearing self-clasping of limbs and head-shaking.

In the study by Chiken et al. (2008), six DYT1 dystonia model (5–28 weeks old, both male and female) and six age-matched normal mice were used. The experimental protocols were approved by the Animal Care and Use Committees of the Mount Sinai School of Medicine and the National Institutes of Natural Sciences, and all experiments were conducted according to the guidelines of the National Institutes of Health Guide for the Care and Use of Laboratory Animals. Each mouse was anesthetized with ketamine hydrochloride (100 mg/kg body weight, i.p.) and xylazine hydrochloride (4–5 mg/kg, i.p.), and fixed in a conventional stereotaxic apparatus. The skull was widely exposed. The exposed skull was completely covered with transparent acrylic resin, and then a small U-frame made of acetal resin for head fixation was mounted and fixed on the head of the mouse.

After recovery from the first surgery (2 or 3 days later), the mouse was positioned in a stereotaxic apparatus with its head restrained using the U-frame head holder under light anesthesia with ketamine hydrochloride (30–50 mg/kg, i.p.). A part of the skull in one hemisphere was removed to access the motor cortex, GPi, and GPe. Two pairs of bipolar stimulating electrodes (tip distance, 300–400 μm) made of 50-μm-diameter Teflon-coated tungsten wires were inserted into the primary motor cortex, one into the caudal forelimb region and the other into the orofacial region. These regions were confirmed by observing movements evoked by intracortical microstimulation. Stimulating electrodes were then fixed therein using acrylic resin.

After full recovery from the second surgery, the mouse was positioned in a stereotaxic apparatus with its head restrained painlessly using the U-frame head holder. The mouse lay down quietly in the awake state. For single unit recording of GPi and GPe neurons, a glass-coated Elgiloy-alloy microelectrode (0.8–1.5 MΩ at 1 kHz) was inserted vertically into the brain through the dura mater using a hydraulic microdrive. Signals from the electrode were amplified, converted to digital pulses using a window discriminator, and sampled using a computer. Spontaneous discharges were recorded, and spontaneous discharge rates and autocorrelograms (bin width of 0.5 ms) of the neurons were calculated from continuous digitized recordings for 30 s. Electrical stimulation of the primary motor cortex (200 μs duration single pulse, 20–50 μA strength), which induced muscle twitches in the corresponding body parts, was delivered. Similar intensities were used for dystonia model and normal mice. Responses to cortical stimulation were examined by constructing peristimulus time histograms (PSTHs; bin width of 1 ms) for 100 stimulus trials.

HUMAN STUDY

In the study by Nishibayashi et al. (2011), one cervical dystonia patient received stereotactic surgery for DBS electrode implantation into the bilateral GPi. The patient was 62-year-old female, and had a disease duration of 32 months, and a Toronto western spasmodic torticollis rating scale (TWSTRS) score of 54. Microelectrode recordings were performed to identify the targets. In addition, 10 Parkinson's disease patients [eight male and two female; mean age, 61.9 years; mean disease duration, 126 months; mean levodopa dosage, 460 mg/day; preoperative unified Parkinson's disease rating scale (UPDRS), 25.3 (best)–66.6 (worst)] were also investigated for comparison. Medications were withdrawn 18 h before operation in most patients. This study was approved by the ethical committee of Wakayama Medical University and followed its guidelines.

Surgery including microelectrode recordings was performed under local anesthesia. Burr holes were made bilaterally on the coronal suture about 30 mm lateral from the midline. After dural incision, a strip electrode with four platinum discs (5-mm-diameter) spaced 10 mm apart (Unique Medical, Tokyo, Japan) was inserted into the subdural space in the posterolateral direction, and placed on the upper limb region of the primary motor cortex ipsilateral to the target GPi. Electrical stimulation (1.0 ms duration single pulse, 1–20 mA strength at 1 Hz) was delivered through two of the four discs. A pair of discs inducing muscle twitches in the contralateral upper limb at the lowest intensity was selected. In the following recordings, stimulation was delivered through this pair at an intensity inducing clear muscle twitches (4–16 mA) at 1 Hz. A microelectrode (FC1002, Medtronic, Minneapolis, MN, USA) was inserted through the same burr hole targeting the tentative target in the posteroventral GPi, which was determined on the basis of magnetic resonance imaging (MRI). Neuronal activity was amplified, displayed (Leadpoint 9033A0315, Medtronic), and fed to a computer for online analysis. The responses induced by electrical stimulation of the cortex were assessed by constructing PSTHs (bin width of 1 ms) for 20–120 stimulus trials. Spontaneous discharge rates and patterns were analyzed from autocorrelograms (bin width of 0.5 ms) constructed from continuous digitized recordings for 50 s. On the basis of the microelectrode recordings, DBS electrodes (Model 3387, Medtronic) were implanted bilaterally into the GPi.

RESULTS

SPONTANEOUS ACTIVITY OF GPi AND GPe NEURONS IN DYT1 DYSTONIA MODEL MICE

GPi (50.6 ± 15.7 Hz, mean ± SD, $n = 94$; **Figure 1A**) and GPe (54.5 ± 16.3 Hz, $n = 70$) neurons in normal mice fired continuously at a high discharge rate. Traces of digitized spikes and autocorrelograms indicated that GPi (**Figures 1A,B**) and GPe neurons fired irregularly in normal mice. On the other hand, the firing frequency of GPi (27.8 ± 19.1 Hz, $n = 90$; **Figure 1C**) and GPe (35.4 ± 19.0 Hz, $n = 204$) neurons in DYT1 dystonia model mice was significantly lower than that in normal mice (**Figure 1E**; $p < 0.001$, Mann–Whitney U test). Discharge patterns also differed in dystonia model mice (**Figures 1C,D**). Bursts and pauses were frequently observed in GPi (thick black lines and thick white lines in **Figure 1C**) and GPe neurons of dystonia model mice.

RESPONSES OF GPi AND GPe NEURONS TO CORTICAL STIMULATION IN DYT1 DYSTONIA MODEL MICE

Cortical stimulation typically evoked a triphasic response composed of early excitation, followed by inhibition, and late excitation in GPi (**Figure 2A**) and GPe neurons of normal mice. On the other hand, the most common response pattern of GPi (56%) and GPe (41%) neurons in dystonia model mice was short-latency monophasic or biphasic excitation followed by long-lasting inhibition (**Figure 2B**), a pattern never observed in normal mice. The duration of the long-lasting inhibition was 73.7 ± 29.4 ms in the GPi ($n = 29$) and 66.7 ± 31.3 ms in the GPe ($n = 46$).

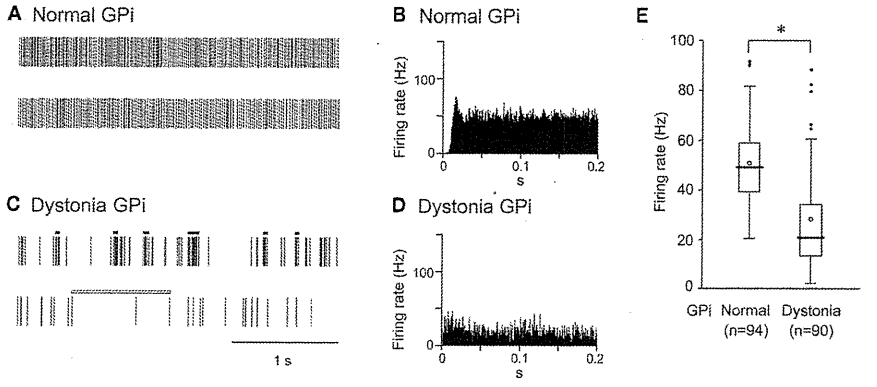

FIGURE 1 | Spontaneous activity of neurons in the internal segment of the globus pallidus (GPi) in DYT1 dystonia model mice. (A,C) Spikes are shown as digital signals in normal **(A)** and dystonia model **(C)** mice. Bursts and pauses in the digital signals are indicated by horizontal black thick lines and horizontal white thick lines, respectively. **(B,D)** Auto-correlograms are shown in normal **(B)** and dystonia model **(D)** mice. **(E)** Box plots of firing rates in normal (left) and dystonia model (right) mice. The boxes are constructed with the top line bounding the upper quartile and the bottom line bounding the lower quartile. The median and mean excluding outliers are indicated by a thick horizontal line and an open circle in the box, respectively. The short horizontal lines show the largest and smallest values that are not outliers. Outliers are shown as small closed circles. *, significantly different ($p < 0.001$, Mann–Whitney U test). Modified from Chiken et al. (2008).

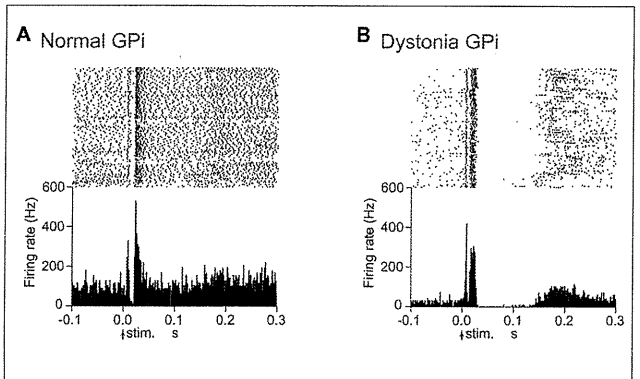

FIGURE 2 | Responses of GPi neurons to cortical stimulation in DYT1 dystonia model mice. (A) Raster and peristimulus time histograms (PSTHs) for normal mice. Cortical stimuli were delivered at time 0 (arrows) for 100 trials. **(B)** Raster and PSTHs for dystonia model mice. Abnormal responses with long-lasting inhibition were observed. Modified from Chiken et al. (2008).

SOMATOTOPIC ORGANIZATION OF THE GPi AND GPe IN DYT1 DYSTONIA MODEL MICE

Stimulation of both forelimb and orofacial regions of the motor cortex was performed. By observing cortically evoked responses, cortical regions projecting to each GPi neuron could be identified. In normal mice, many neurons responded to stimulation of the forelimb region, and a small number of neurons responded to stimulation of the orofacial region (**Figure 3A**). The number of neurons with convergent inputs from both forelimb and orofacial regions was small (7%). On the other hand, the number of GPi neurons with convergent inputs was increased in dystonia model mice (28%).

The locations of recorded GPi neurons are plotted on the basis of cortical inputs in **Figure 3B**. In the GPi of normal mice, the neurons with forelimb inputs were distributed over a wide area of the GPi, although not in its most medial portion (**Figure 3B** top). A few neurons with orofacial inputs were found in the lateral portion of the GPi. In dystonia model mice, however, such a segregation disappeared. The number of GPi neurons with orofacial inputs and those with convergent inputs was increased, and they intruded into the central portion of the GPi, although the most medial portion remained unresponsive (**Figure 3B** bottom). Similar changes were also observed in the GPe. These observations suggest that somatotopic arrangements are disorganized in the GPi and GPe of dystonia model mice.

ACTIVITY OF GPi AND GPe NEURONS IN A HUMAN CERVICAL DYSTONIA PATIENT

Neurons were recorded mostly in motor territories of the GPi and GPe. The firing rates of GPi (62.3 ± 12.1 Hz, $n = 9$) and GPe (45.8 ± 17.6 Hz, $n = 11$) neurons in a cervical dystonia patient were significantly lower than those of GPi (92.7 ± 40.1 Hz, $n = 34$) and GPe (81.0 ± 52.5 Hz, $n = 17$) neurons in Parkinsonian patients ($p < 0.05$, t-test). Most GPi and GPe neurons of a cervical dystonia patient showed burst (6/9 GPi and 5/11 GPe) or oscillatory (1–4 Hz) burst (1/9 GPi and 6/11 GPe) activity (**Figure 4A**). More than one-third of recorded neurons (6/13 GPi and 4/11 GPe in a cervical dystonia patient and 21/68 GPi and 18/45 GPe in Parkinsonian patients) showed responses to cortical stimulation. These GPi and GPe neurons were considered to be located in the upper limb regions of the GPi and GPe, because these neurons often responded to sensory stimulation of the upper limb. In Parkinsonian patients, response patterns to cortical stimulation were combinations of early excitation, inhibition, and late excitation (data not shown). On the other hand, in a cervical dystonia patient, long-lasting inhibition preceded by excitation (**Figure 4B**) and long-lasting monophasic inhibition (**Figure 4C**) were the typical response patterns. These response patterns are very similar to those observed in dystonia model mice (compare **Figures 4B,C** with **Figure 2B**).

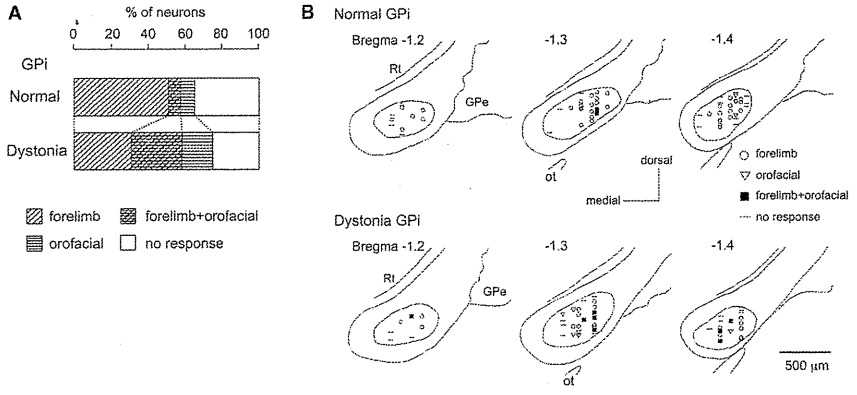

FIGURE 3 | Somatotopic organization in the GPi of DYT1 dystonia model mice. (A) Proportions of neurons classified on the basis of cortical inputs in normal (top) and dystonia model (bottom) mice. **(B)** Distribution of recorded GPi neurons indicated by symbols on the basis of cortical inputs. Data from normal (top) and dystonia model (bottom) mice are shown in frontal sections. Figures in the left upper corner represent distance from bregma. GPe, external segment of the globus pallidus; Rt, reticular thalamic nucleus; Ot, optic tract. Modified from Chiken et al. (2008).

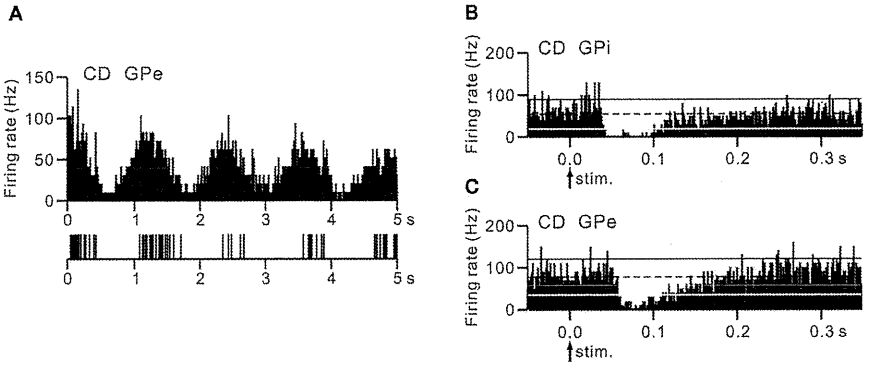

FIGURE 4 | Activity of GPi and GPe neurons in a human cervical dystonia patient. (A) Autocorrelograms and slow traces of digitized spikes of GPe neurons recorded from a cervical dystonia (CD) patient. **(B,C)** PSTHs (bin width of 1 ms) showing the responses of GPi **(B)** and GPe **(C)** neurons evoked by stimulation of the upper limb region of the primary motor cortex in a cervical dystonia patient. Cortical stimuli were delivered at time 0 (arrows) for 100 trials. The mean firing rate is indicated by black dotted lines. The statistical levels of $p < 0.05$ (one-tailed *t*-test) calculated from the firing rate during 100 ms preceding the onset of stimulation are indicated by black and white solid lines (upper and lower limits of $p < 0.05$). Modified from Nishibayashi et al. (2011).

DISCUSSION

The first part of the present article characterized the electrophysiological properties of transgenic mice developed to express human ΔE-torsinA as a model of DYT1 dystonia. These mice exhibited: (1) decreased GPi and GPe activity with bursts and pauses, (2) cortically evoked long-lasting inhibition in the GPi and GPe, and (3) somatotopic disorganization in the GPi and GPe. In the second part, similar activity changes, such as decreased activity with bursts and cortically evoked long-lasting inhibition, were also observed in the GPi and GPe of a human cervical dystonia patient. These neuronal abnormalities may be responsible for the symptoms observed in dystonia.

DECREASED GPi AND GPe ACTIVITY IN DYSTONIA

In the present article, reduction of the spontaneous firing rates of GPi and GPe neurons was observed in dystonia model mice and a human cervical dystonia patient. Alteration of firing patterns was also observed in both of them, including bursting discharges and pauses. Decreased discharge rates and irregularly grouped discharges with intermittent pauses in GPi and GPe neurons were also reported in patients with generalized dystonia (Vitek et al., 1999; Zhuang et al., 2004; Starr et al., 2005) and cervical dystonia (Tang et al., 2007). Dystonic hamsters with paroxysmal generalized dystonia also exhibited reduced and bursting GPi activity (Gernert et al., 2002). The correlation between abnormal neuronal activity and abnormal movements was not investigated in the present mice study, because it was difficult to observe abnormal movements under head fixation. The mechanisms responsible for decreased firing rates may include: (1) alteration of membrane properties of GPi and GPe neurons, (2) increased inhibitory inputs to the GPi and GPe, such as GABAergic inputs from the striatum, and/or (3) decreased excitatory inputs to the GPi and

GPe, such as glutamatergic inputs from the subthalamic nucleus (STN). Inhibitory inputs from the striatum to the GPi and GPe were increased in dystonia model mice as discussed in the next section.

CORTICALLY EVOKED LONG-LASTING INHIBITION IN GPi AND GPe NEURONS OF DYSTONIA

In normal mice, cortical stimulation typically induced triphasic responses composed of early excitation, inhibition, and late excitation in GPi and GPe neurons. Similar triphasic responses were also observed in the GPi and GPe of rats and monkeys. The origin of each component has been intensively studied (Ryan and Clark, 1991; Maurice et al., 1998, 1999; Nambu et al., 2000; Kita et al., 2004; Tachibana et al., 2008). Early excitation is mediated by the cortico-STN-GPe/GPi pathway, while inhibition and late excitation are mediated by the cortico-striato-GPe/GPi and cortico-striato-GPe-STN-GPe/GPi pathways, respectively.

On the other hand, in dystonia model mice we examined, cortical stimulation induced early excitation followed by late long-lasting inhibition in GPi and GPe neurons. Similar response patterns were induced in GPi and GPe neurons of a human cervical dystonia patient. These abnormal patterns of responses may be generated through the cortico-basal ganglia pathways. The early excitation seems to be mediated, at least in its early phase, by the cortico-STN-GPe/GPi pathway, as in normal mice, since the latency of the early excitation in dystonia model mice was short and similar to that in normal mice. The origin of the late long-lasting inhibition may be (1) increased inhibitory input via the striato-GPe/GPi pathway, or (2) decreased excitatory input via the STN-GPe/GPi pathway. The latter explanation seems less likely to be correct, since our preliminary observation indicates that the spontaneous activity of STN neurons is unchanged in dystonia model mice. Thus, increased activity through both cortico-striato-GPi *direct* and cortico-striato-GPe *indirect* pathways is considered to be the fundamental change in dystonia. The above observations also suggest that spontaneous excitation in the cortex that is transmitted to the GPi and GPe through the cortico-basal ganglia pathways could also induce short-latency excitation and long-lasting inhibition, which might be the origins of bursts and pauses, respectively.

SOMATOTOPIC DISORGANIZATION IN THE GPi AND GPe OF DYSTONIA

The somatotopic organization in the GPi and GPe was observed in normal mice as well as monkeys (DeLong et al., 1985; Yoshida et al., 1993). On the other hand, in dystonia model mice, somatotopic arrangements were disorganized, and many GPi and GPe neurons received convergent inputs from both forelimb and orofacial regions. Widened somatosensory receptive fields in pallidal neurons were reported in patients with generalized (Vitek et al., 1999) and focal (Lenz et al., 1998; Sanger et al., 2001) dystonia. Interference of information processing may occur through the cortico-basal ganglia pathways. One explanation for this could be that each single GPi or GPe neuron receives inputs from more striatal neurons in dystonia model mice than in normal mice. Such an explanation agrees well with the hypothesis that in dystonia, inhibition in the GPi/GPe is increased through the striato-GPe/GPi pathways as described in the previous section.

PATHOPHYSIOLOGY OF DYSTONIA

The GPi, the output nucleus of the basal ganglia, is composed of GABAergic inhibitory neurons and fires at high frequency in normal states. Its target structures, such as the thalamus and frontal cortex, are thus continuously inhibited. Striatal inputs reduce GPi activity in a temporal fashion, excite thalamic and cortical neurons through disinhibitory mechanism, and finally release appropriate movements with appropriate timing (**Figure 5A**; Nambu et al., 2000, 2002). On the other hand, in dystonia model mice and a human cervical dystonia patient, cortical excitation induced long-lasting inhibition in the GPi (**Figure 5B**). This suggests that even tiny amounts of spontaneous or voluntary neuronal activity originating in the cortex are transmitted through the cortico-basal ganglia pathways to induce strong, long-lasting inhibition in the GPi. Moreover, somatotopic disorganization was noted in the GPi of dystonia, and cortical activation could induce inhibition over a wide area of the GPi. Reduced GPi output may activate wide areas of the thalamus and cortex in an uncontrollable fashion, resulting in the involuntary movements observed in dystonia. In a similar manner, the cortical areas controlling agonist and antagonist muscles are concurrently activated, and co-contraction of agonist and antagonist muscles could be induced. This may also explain the "motor overflow" that is unintentional muscle contraction during voluntary movements in dystonia. Activation of the upper limb region in the motor cortex, for example, may inhibit large areas of the GPi and finally induce involuntary movements of multiple body parts (**Figure 5B**).

CONCLUSION

The activity of GPi and GPe neurons in DYT1 dystonia model mice and a human cervical dystonia patient was investigated. Both of them showed similar activity changes, such as decreased spontaneous activity with bursts and long-lasting inhibition evoked by cortical stimulation, indicating increased activity through

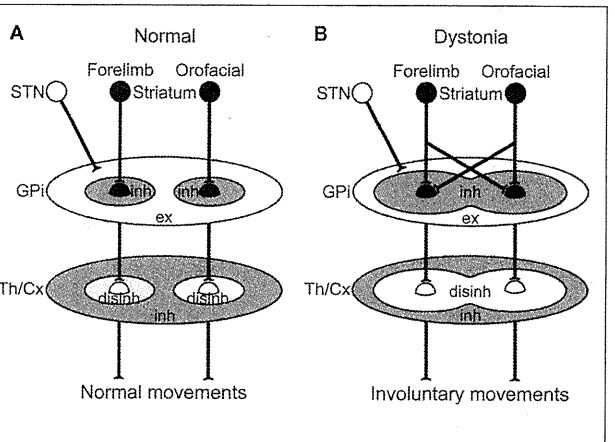

FIGURE 5 | Schematic diagrams showing information processing through the basal ganglia in normal (A) and dystonia (B) conditions. In dystonia **(B)**, cortical activation induces strong inhibition over a wide area of the GPi. Reduced GPi output may cause strong excitation in the thalamus (Th) and cortex (Cx) through disinhibitory mechanism, resulting in the involuntary movements. disinh, disinhibition; ex, excitation; inh, inhibition; STN, subthalamic nucleus. Modified from Chiken et al. (2008).

the cortico-striato-GPi *direct* and cortico-striato-GPe *indirect* pathways. Such a mechanism may explain the pathophysiology of dystonia: Neuronal activity originating in the cortex is transmitted through the cortico-basal ganglia pathways to induce strong, long-lasting inhibition in the GPi. Reduced GPi output may cause increased thalamic and cortical activity, resulting in the involuntary movements.

ACKNOWLEDGMENTS

The animal study was supported by a Grants-in-Aid for Exploratory Research (18650089) and a Grants-in-Aid for Scientific Research (B) (18300135) from the Ministry of Education, Culture, Sports, Science, and Technology of Japan (MEXT), The Uehara Memorial Foundation, Takeda Science Foundation, and United States–Japan Brain Research Cooperative Program (Atsushi Nambu); a Grants-in-Aid for Scientific Research (C) (19500354) from MEXT (Satomi Chiken); and National Institute of Neurological Disorders and Stroke-National Institutes of Health Grant (NS-043038) (Pullanipally Shashidharan). The human study was supported by Wakayama Foundation for the Promotion of Medicine (Toru Itakura), a Grants-in-Aid for Scientific Research (B) (18300135) from MEXT and the Uehara Memorial Foundation (Atsushi Nambu), and NIH grants (NS-47085 and NS-57236) (Hitoshi Kita).

REFERENCES

Chiken, S., Shashidharan, P., and Nambu, A. (2008). Cortically evoked long-lasting inhibition of pallidal neurons in a transgenic mouse model of dystonia. *J. Neurosci.* 28, 13967–13977.

Chiken, S., and Tokuno, H. (2003). Ablation of striatal interneurons influences activities of entopeduncular neurons. *Neuroreport* 14, 675–678.

DeLong, M. R., Crutcher, M. D., and Georgopoulos, A. P. (1985). Primate globus pallidus and subthalamic nucleus: functional organization. *J. Neurophysiol.* 53, 530–543.

Gernert, M., Bennay, M., Fedrowitz, M., Rehders, J. H., and Richter, A. (2002). Altered discharge pattern of basal ganglia output neurons in an animal model of idiopathic dystonia. *J. Neurosci.* 22, 7244–7253.

Kita, H., Nambu, A., Kaneda, K., Tachibana, Y., and Takada, M. (2004). Role of ionotropic glutamatergic and GABAergic inputs on the firing activity of neurons in the external pallidum in awake monkeys. *J. Neurophysiol.* 92, 3069–3084.

Lenz, F. A., Suarez, J. I., Metman, L. V., Reich, S. G., Karp, B. I., Hallett, M., Rowland, L. H., and Dougherty, P. M. (1998). Pallidal activity during dystonia: somatosensory reorganisation and changes with severity. *J. Neurol. Neurosurg. Psychiatr.* 65, 767–770.

Maurice, N., Deniau, J. M., Glowinski, J., and Thierry, A. M. (1998). Relationships between the prefrontal cortex and the basal ganglia in the rat: physiology of the corticosubthalamic circuits. *J. Neurosci.* 18, 9539–9546.

Maurice, N., Deniau, J. M., Glowinski, J., and Thierry, A. M. (1999). Relationships between the prefrontal cortex and the basal ganglia in the rat: physiology of the cortico-nigral circuits. *J. Neurosci.* 19, 4674–4681.

Nambu, A., Tokuno, H., Hamada, I., Kita, H., Imanishi, M., Akazawa, T., Ikeuchi, Y., and Hasegawa, N. (2000). Excitatory cortical inputs to pallidal neurons via the subthalamic nucleus in the monkey. *J. Neurophysiol.* 84, 289–300.

Nambu, A., Tokuno, H., and Takada, M. (2002). Functional significance of the cortico-subthalamo-pallidal 'hyperdirect' pathway. *Neurosci. Res.* 43, 111–117.

Nishibayashi, H., Ogura, M., Kakishita, K., Tanaka, S., Tachibana, Y., Nambu, A., Kita, H., and Itakura, T. (2011). Cortically evoked responses of human pallidal neurons recorded during stereotactic neurosurgery. *Mov. Disord.* 26, 469–476.

Ozelius, L. J., Hewett, J. W., Page, C. E., Bressman, S. B., Kramer, P. L., Shalish, C., de Leon, D., Brin, M. F., Raymond, D., Corey, D. P., Fahn, S., Risch, N. J., Buckler, A. J., Gusella, J. F., and Breakefield, X. O. (1997). The early-onset torsion dystonia gene (DYT1) encodes an ATP-binding protein. *Nat. Genet.* 17, 40–48.

Ryan, L. J., and Clark, K. B. (1991). The role of the subthalamic nucleus in the response of globus pallidus neurons to stimulation of the prelimbic and agranular frontal cortices in rats. *Exp. Brain Res.* 86, 641–651.

Sanger, T. D., Tarsy, D., and Pascual-Leone, A. (2001). Abnormalities of spatial and temporal sensory discrimination in writer's cramp. *Mov. Disord.* 16, 94–99.

Shashidharan, P., Sandu, D., Potla, U., Armata, I. A., Walker, R. H., McNaught, K. S., Weisz, D., Sreenath, T., Brin, M. F., and Olanow, C. W. (2005). Transgenic mouse model of early-onset DYT1 dystonia. *Hum. Mol. Genet.* 14, 125–133.

Starr, P. A., Rau, G. M., Davis, V., Marks, W. J. Jr., Ostrem, J. L., Simmons, D., Lindsey, N., and Turner, R. S. (2005). Spontaneous pallidal neuronal activity in human dystonia: comparison with Parkinson's disease and normal macaque. *J. Neurophysiol.* 93, 3165–3176.

Tachibana, Y., Kita, H., Chiken, S., Takada, M., and Nambu, A. (2008). Motor cortical control of internal pallidal activity through glutamatergic and GABAergic inputs in awake monkeys. *Eur. J. Neurosci.* 27, 238–253.

Tang, J. K., Moro, E., Mahant, N., Hutchison, W. D., Lang, A. E., Lozano, A. M., and Dostrovsky, J. O. (2007). Neuronal firing rates and patterns in the globus pallidus internus of patients with cervical dystonia differ from those with Parkinson's disease. *J. Neurophysiol.* 98, 720–729.

Vitek, J. L., Chockkan, V., Zhang, J. Y., Kaneoke, Y., Evatt, M., DeLong, M. R., Triche, S., Mewes, K., Hashimoto, T., and Bakay, R. A. E. (1999). Neuronal activity in the basal ganglia in patients with generalized dystonia and hemiballismus. *Ann. Neurol.* 46, 22–35.

Yoshida, S., Nambu, A., and Jinnai, K. (1993). The distribution of the globus pallidus neurons with input from various cortical areas in the monkeys. *Brain Res.* 611, 170–174.

Zhuang, P., Li, Y., and Hallett, M. (2004). Neuronal activity in the basal ganglia and thalamus in patients with dystonia. *Clin. Neurophysiol.* 115, 2542–2557.

Conflict of Interest Statement: The authors declare that the research was conducted in the absence of any commercial or financial relationships that could be construed as a potential conflict of interest.

Received: 21 April 2011; accepted: 18 October 2011; published online: 28 November 2011.

Citation: Nambu A, Chiken S, Shashidharan P, Nishibayashi H, Ogura M, Kakishita K, Tanaka S, Tachibana Y, Kita H and Itakura T (2011) Reduced pallidal output causes dystonia. Front. Syst. Neurosci. 5:89. doi: 10.3389/fnsys.2011.00089

J Neuropathol Exp Neurol

Vol. 70, No. 8
August 2011
pp. 686–697

ORIGINAL ARTICLE

Parkin-Mediated Protection of Dopaminergic Neurons in a Chronic MPTP-Minipump Mouse Model of Parkinson Disease

Toru Yasuda, PhD, Hideki Hayakawa, PhD, Tomoko Nihira, DMC, Yong-Ri Ren, PhD, Yasuto Nakata, MSc, Makiko Nagai, MD, PhD, Nobutaka Hattori, MD, PhD, Koichi Miyake, MD, PhD, Masahiko Takada, MD, PhD, Takashi Shimada, MD, PhD, Yoshikuni Mizuno, MD, PhD, and Hideki Mochizuki, MD, PhD

Abstract

Loss-of-function mutations in the ubiquitin ligase parkin are the major cause of recessively inherited early-onset Parkinson disease (PD). Impairment of parkin activity caused by nitrosative or dopamine-related modifications may also be responsible for the loss of dopaminergic (DA) neurons in sporadic PD. Previous studies have shown that viral vector-mediated delivery of parkin prevented DA neurodegeneration in several animal models, but little is known about the neuroprotective actions of parkin in vivo. Here, we investigated mechanisms of neuroprotection of overexpressed parkin in a modified long-term mouse model of PD using osmotic minipump administration of 1-methyl-4-phenyl-1,2,3,6-tetrahydropyridine (MPTP). Recombinant adeno-associated viral vector-mediated intranigral delivery of parkin prevented motor deficits and DA cell loss in the mice. Ser129-phosphorylated α-synuclein–immunoreactive cells were increased in the substantia nigra of parkin-treated mice. Moreover, delivery of parkin alleviated the MPTP-induced decrease of the active phosphorylated form of Akt. On the other hand, upregulation of p53 and mitochondrial alterations induced by chronic MPTP administration were barely suppressed by parkin. These results suggest that the neuroprotective actions of parkin may be impaired in severe PD.

From the Department of Neurology (TY, HH, TN, YRR, YN, MN, YM, HM), and Division of Neuroregenerative Medicine (YM), Kitasato University School of Medicine, Minami-ku, Sagamihara, Kanagawa, Japan; Department of Neurology, and Research Institute for Diseases of Old Age (TY, HH, TN, YRR, NH, YM, HM), Juntendo University School of Medicine, Bunkyo-ku, Tokyo, Japan; Department of Biochemistry and Molecular Biology (KM, TS), Division of Gene Therapy Research, Center for Advanced Medical Technology, Nippon Medical School, Bunkyo-ku, Tokyo, Japan; and Systems Neuroscience Section (MT), Department of Cellular and Molecular Biology, Primate Research Institute, Kyoto University, Inuyama, Aichi, Japan.

Send correspondence and reprint requests to: Hideki Mochizuki, MD, PhD, Department of Neurology, Kitasato University School of Medicine, 1-15-1 Kitasato, Minami-ku, Sagamihara, Kanagawa 252-0374, Japan; E-mail: hmoc0823@med.kitasato-u.ac.jp

This work was supported by the Program for Promotion of Fundamental Studies in Health Sciences of the National Institute of Biomedical Innovation; Grants-in-Aid from the Research Committee of CNS Degenerative Diseases, the Ministry of Health, Labour and Welfare of Japan (to H.M.); the Research Grant for Longevity Sciences from the Ministry of Health, Labour and Welfare of Japan (to H.M.); and grants (No. S0801035) from the Ministry of Education, Culture, Sports, Science, and Technology of Japan (to H.M.).

Supplemental digital content is available for this article. Direct URL citations appear in the printed text and are provided in the HTML and PDF versions of this article on the journal's Web site (www.jneuropath.com).

Key Words: α-Synuclein, Adeno-associated virus, MPTP, Neuroprotection, Osmotic minipump, Parkin, Parkinson disease.

INTRODUCTION

Parkinson disease (PD) is a progressive neurodegenerative disorder characterized clinically by resting tremor, rigidity, akinesia, and postural instability (1). The pathologic hallmarks of PD are loss of dopaminergic (DA) neurons in the substantia nigra (SN) pars compacta (SNpc) and intraneuronal protein inclusions termed *Lewy bodies*, which are composed mainly of α-synuclein (αSyn) (2). Both environmental and genetic factors are considered to be involved in PD pathogenesis (1, 3). Sporadic cases represent more than 90% of total patients with PD, but there are several inherited forms caused by mutations in single genes (1). Among these familial forms of PD, approximately 50% of recessively inherited early-onset parkinsonism is caused by loss-of-function mutations in the parkin gene *PARK2* (4).

PARK2 encodes a 465-amino acid protein that functions as a ubiquitin ligase (5). Most PARK2 patients seem to lack Lewy bodies (6–9), suggesting an important role for parkin in Lewy body formation (10). Several putative substrates of parkin have been reported and can be divided into 2 subgroups: those that are destined for proteasomal degradation by receiving canonical K48-linked polyubiquitination (11) and others that acquire multiple physiological or pathophysiological functions by receiving monoubiquitination or K63-linked polyubiquitination. The latter may be involved in inclusion formation (12–16). In animal models, loss of parkin increases mitochondrial dysfunction and oxidative damage (17), impairment of evoked dopamine release (18), and vulnerability to inflammation-related neurodegenerative insult (19). *S*-Nitrosylation or covalent binding of dopamine-related compounds may be responsible for parkin inactivation and subsequent DA cell death in sporadic PD (20–22). Moreover, there is increasing evidence that ectopically overexpressed parkin provides neuroprotective effects in genetic and environmental PD models, including *LRRK2*-transgenic (23) and *PINK1*-knockdown fruit flies (24), 6-hydroxydopamine–lesioned rats (25), and mice treated transiently with 1-methyl-4-phenyl-1,2,3,6-tetrahydropyridine (MPTP) (26). We previously reported that recombinant adeno-associated viral (rAAV) vector-mediated delivery of parkin

prevented αSyn-induced DA neuronal loss in rat and monkey brains (27, 28).

Recent studies indicate that there are functional interactions of parkin with PINK1, which is involved in mitochondrial quality control (29–33). However, the neuroprotective actions of parkin against long-term mitochondrial insult are relatively unknown in vivo. This study was designed to dissect the parkin-mediated neuroprotection in a long-term environmental model of PD. We generated modified high-dose and long-term MPTP mice using Alzet osmotic minipumps and investigated the impact of rAAV-mediated parkin delivery.

MATERIALS AND METHODS

Mice

Normal male C57BL/6J mice were purchased from Charles River Laboratories (Kanagawa, Japan). All experimental protocols were approved by the Ethics Review Committee for Animal Experimentation of Juntendo University and by the Animal Experimentation and Ethics Committee of the Kitasato University School of Medicine.

Preparation of rAAV Vector

The plasmid pAAV-MCS (CMV promoter; Stratagene, La Jolla, CA) carrying human *parkin* complementary DNA (named pAAV-MCS-parkin) or human *αSyn* complementary DNA (pAAV-MCS-αSyn) was constructed as previously reported (27, 34). High-titer serotype-1 rAAV (rAAV1) vector stocks were prepared using the plasmid pAAV-MCS-parkin, pAAV-MCS-αSyn, or pAAV-hrGFP (humanized recombinant green fluorescent protein; Stratagene), as described (28, 35). The rAAV1 vectors were purified by ultracentrifugation in a gradient density of OptiPrep solution (Axis-Shield PoC AS, Oslo, Norway), which was then removed by ultrafiltration using Centricon Plus-20 (10,000 MWCO; Millipore Corp, Temecula, CA). The titers of rAAV1 to produce parkin (named rAAV1-parkin), αSyn (rAAV1-αSyn), or hrGFP (rAAV1-hrGFP) were 5×10^{11} genomes per milliliter.

Stereotaxic Injection of rAAV1 Vectors

Mice were anesthetized with sodium pentobarbital (50 mg/kg body weight, intraperitoneally [i.p.]) and positioned in a stereotaxic frame. For immunohistochemistry (IHC) and measurement of the striatal dopamine and its metabolites, rAAV1 vector was injected unilaterally. For Western blotting, the rAAV1 vector was injected bilaterally. The skull was exposed, and a small portion of the skull over the SN was removed with a dental drill. Subsequently, the rAAV1 vector was injected into the SN (2 μL; 2.8 mm posterior and 1.3 mm lateral from the bregma, 4.4 mm below the dural surface; tooth bar = −2 mm) through a 5-μL Hamilton microsyringe, as previously described (35).

MPTP Infusion

The 13-week-old mice (~30 g body weight) were implanted i.p. with the Alzet osmotic minipumps (Model 2004, releasing rate = 0.25 μL/h, reservoir volume = 200 μL; Durect Corp, Cupertino, CA), filled with saline (control group), 250 mg/mL MPTP-HCl (50-mg/kg-per-day group; dissolved in saline; Sigma-Aldrich Corp, St Louis, MO), or 500 mg/mL MPTP-HCl (100-mg/kg-per-day group). For bolus injection, mice were injected i.p. with MPTP at 30 mg/kg per day for 5 consecutive days (designated as subacute; n = 4).

For rAAV1-injected mice, the same Alzet minipumps filled with saline (control group) or 250 mg/mL MPTP-HCl (50-mg/kg-per-day group) were implanted at 14 days after injection of the rAAV1 vectors. MPTP was handled in accordance with guidelines reported by Przedborski et al (36).

Behavioral Analysis

To evaluate behavioral changes, the mice were analyzed by a rotarod test 25 days after implantation of the osmotic minipump (i.e. 3 days before death). Mice were kept for 300 seconds twice on a rotarod apparatus accelerating from 0 to 32 rpm at 45-minute intervals (Model 7650, rota-rod for mice; Ugo Basile Biological Research Apparatus, Comerio VA, IT). The latency times (seconds) to fall were measured by accelerating from 0 to 32 rpm in 300 seconds.

rAAV1-injected mice were analyzed by apomorphine-induced rotation test 25 days after the minipump implantation (3 days before death). Mice were habituated in a circular chamber (16 cm in diameter) for 10 minutes. Then, after the injection of apomorphine-HCl (0.5 mg/kg i.p., dissolved in saline containing 30% ascorbic acid; Sigma-Aldrich Corp), rotation behavior was monitored for 40 minutes using a video recorder. In a previous report, apomorphine-challenged rats rotated toward the side with weaker DA neurotransmission (37), and the number of contralateral full body turns was

TABLE. Numbers of Mice Used for rAAV1 Injection Experiments

Immunohistochemistry and Other Studies	**Unilateral Injection of rAAV1 Vectors; Killed 28 Days After Minipump Implantation**			
Group	rAAV1-hrGFP/saline	rAAV1-parkin/saline	rAAV1-hrGFP/MPTP	rAAV1-parkin/MPTP
No. mice analyzed/injected	4/4	4/4	4/6	5/6
Western	**Bilateral Injection of rAAV1 Vectors; Killed 7 Days After Minipump Implantation**			
Group	rAAV1-hrGFP/saline	rAAV1-parkin/saline	rAAV1-hrGFP/MPTP	rAAV1-parkin/MPTP
No. mice analyzed/injected	4/4	4/4	4*/6	4*/6

Numbers of mice injected with the rAAV1 vector (injected) and used for data analyses (analyzed) are shown. For immunohistochemistry and measurements of dopamine and its metabolites, mice that exhibited foreign protein expression in more than ~80% of the area of the entire rostrocaudal region of the substantia nigra pars compacta were used for the analyses. In Western blotting analysis, the protein samples that showed an intense foreign protein expression were used for the analyses.

*One mouse died before minipump implantation.

hrGFP, humanized recombinant green fluorescent protein; MPTP, 1-methyl-4-phenyl-1,2,3,6-tetrahydropyridine; rAAV1, recombinant adeno-associated viral vector 1.

counted by playing back the recorded videotape. A full-body turn was defined as continuous and pivotal turning exceeding 180 degrees.

Tissue Processing

At 7 or 28 days after implantation of the minipumps, or 25 days after the first injection of MPTP (subacute group), mice were deeply anesthetized with sodium pentobarbital (250 mg/kg, i.p.) and perfused transcardially with phosphate-buffered saline (PBS). The brains were removed en bloc from the skull and cut coronally along the anterior tangent to the median eminence. The striatal tissues were then dissected and immediately frozen on dry ice. For Western blotting, the brain blocks including the entire rostrocaudal extent of the SN were cut coronally at 2-mm thickness (Figure, Supplemental Digital Content 1, parts A, B, http://links.lww.com/NEN/A252). After removal of the cortical and hippocampal tissues, the ventral midbrains were cut horizontally along the ventral end close to the SN to remove the tissues including the median eminence and pontine nucleus. Then, ventral parts of midbrain tissues (~1.2 mm from the ventral end) were dissected horizontally, from which the ventrolateral tissues including SN pars reticulata were removed (Figure, Supplemental Digital Content 1, parts A, B, http://links.lww.com/NEN/A252), and immediately frozen on dry ice. For IHC, the posterior parts of brain blocks, including the entire rostrocaudal extent of the SN, were fixed overnight in 4% paraformaldehyde in PBS and immersed in PBS containing 30% sucrose until sinking. Coronal sections of the SN were cut serially at 20-μm thickness by a cryostat (CM1900; Leica Microsystems, Wetzlar, Germany).

The rAAV1-αSyn-injected (n = 3) and rAAV1-hrGFP-injected mice (n = 3) were killed at 4 weeks after injection. Brain tissues including the entire rostrocaudal extent of the SN were fixed overnight in 4% paraformaldehyde in PBS and processed for IHC as described previously.

Antibodies

The primary antibodies used for IHC were rabbit anti-hrGFP (diluted at 1:500; Stratagene), rabbit anti-parkin (no. 2132; 1:500; Cell Signaling Technology, Inc, Danvers, MA), mouse anti-parkin (no. 4211, clone Park8; 1:200; Cell Signaling Technology), mouse anti-tyrosine hydroxylase (TH) (1:10000; Calbiochem, San Diego, CA), rabbit anti-TH (1:5000; Calbiochem), sheep anti-TH (1:1000; Calbiochem), mouse anti-glial fibrillary acidic protein (clone ab10062; 1:500; Abcam, Cambridge, MA), mouse anti-human αSyn (clone LB509; 1:200; Invitrogen Corp, Carlsbad, CA), rabbit anti–Ser129-phosphorylated αSyn (clone ab59264; 1:500; Abcam), and rabbit anti-translocase of the outer membrane 20 (Tom20) antibodies (FL-145; 1:500; Santa Cruz Biotechnology, Inc, Santa Cruz, CA).

The primary antibodies used for Western blotting were as follows: rabbit anti-hrGFP (1:500), mouse anti-parkin (1:500), rabbit anti–phospho-Akt (Ser473) (no. 4060, clone D9E; 1:1000; Cell Signaling Technology), rabbit anti-Akt (no. 9272; 1:500; Cell Signaling Technology), mouse anti-p53 (Pab 1801; 1:100; Santa Cruz Biotechnology), mouse anti-Bax (B-9; 1:100; Santa Cruz Biotechnology), mouse anti–phospho-stress-activated protein kinase/c-Jun N-terminal kinase (JNK) (Thr183/Tyr185) (no. 9255, clone G9; 1:1000; Cell Signaling Technology), mouse anti-TH (1:500; Calbiochem), rabbit anti-PINK1 (NB100-493; 1:500; Novus Biologicals, Littleton, CO), rabbit anti-DJ-1 (NB100-483; 1:500;

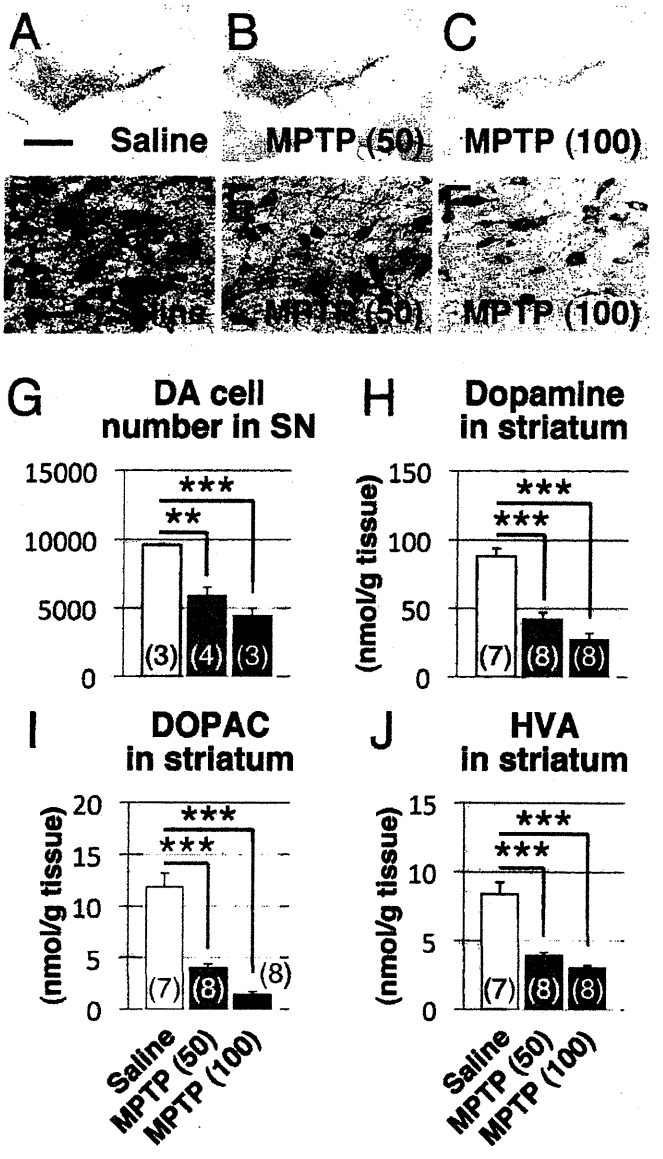

FIGURE 1. Long-term and high-dose MPTP models generated using Alzet osmotic minipumps. **(A–F)** Substantia nigra (SN) sections of saline- (Saline) and MPTP-minipump mice (50 mg/kg per day, MPTP [50] or 100 mg/kg per day MPTP [100]) immunostained for tyrosine hydroxylase (TH) and counterstained with Cresyl violet. **(G–J)** Numbers of dopaminergic (DA) cell bodies in the SN pars compacta **(G)**, and levels of dopamine **(H)**, 2-(3,4-dihydroxyphenyl)acetic acid (DOPAC) **(I)**, and homovanillic acid (HVA) in the striatum **(J)**. The implantation of MPTP-minipump caused a significant degeneration of the nigrostriatal DA neurons. Numbers of mice analyzed in each group are indicated within the bars. Data are mean ± SEM. **, $p < 0.01$; and ***, $p < 0.001$ (1-way analysis of variance followed by Tukey-Kramer post hoc test). Scale bars = **(A)** 500 μm (applicable to **A–C**); **(D)** 50 μm **(D–F)**.

Novus Biologicals), rabbit anti-Tom20 (FL-145; 1:200; Santa Cruz Biotechnology), rabbit anti-Ser129-phosphorylated αSyn (clone ab42906; 1:500; Abcam), mouse anti–Ser129-phosphorylated αSyn (clone pSyn#64; 1:1000; Wako Pure Chemical Industries, Ltd, Osaka, Japan), mouse anti-αSyn (clone 42; 1:500; BD Biosciences, Franklin Lakes, NJ), and mouse anti-actin antibodies (clone C4; 1:500; Millipore Corp).

Immunohistochemistry

Free-floating sections were washed in a PBS medium containing 0.05% Triton X-100 (PBS-T). When the rabbit and sheep primary antibodies were used, the sections were soaked with 10% Block Ace (Yukijirushi-Nyugyo Co, Sapporo, Japan) in PBS-T and then incubated with the primary antibodies dissolved in PBS-T containing 2% Block Ace at 4°C for 48 hours. When the mouse primary antibody was used, Vector M.O.M. Immunodetection Kit (Vector Laboratories, Inc, Burlingame, CA) was used for blocking and antibody dilution according to the instructions provided by the manufacturer. Subsequently, for fluorescent visualization of the antigens, the sections were incubated for 2 hours in fresh medium containing fluorescein isothiocyanate–conjugated anti-mouse or rabbit IgG and Cy3-conjugated anti-mouse, rabbit, or sheep IgG secondary antibodies (1:200–500; Jackson ImmunoResearch Laboratories, Inc, West Grove, PA). The sections were mounted on slide glass and coverslipped with Vectashield Mounting Medium with DAPI (Vector Laboratories). Images were captured using a confocal laser scanning microscope (LSM510; Zeiss, Jena, Germany). For colorimetric visualization of the antigen, the sections were incubated for 2 hours in fresh medium containing biotinylated

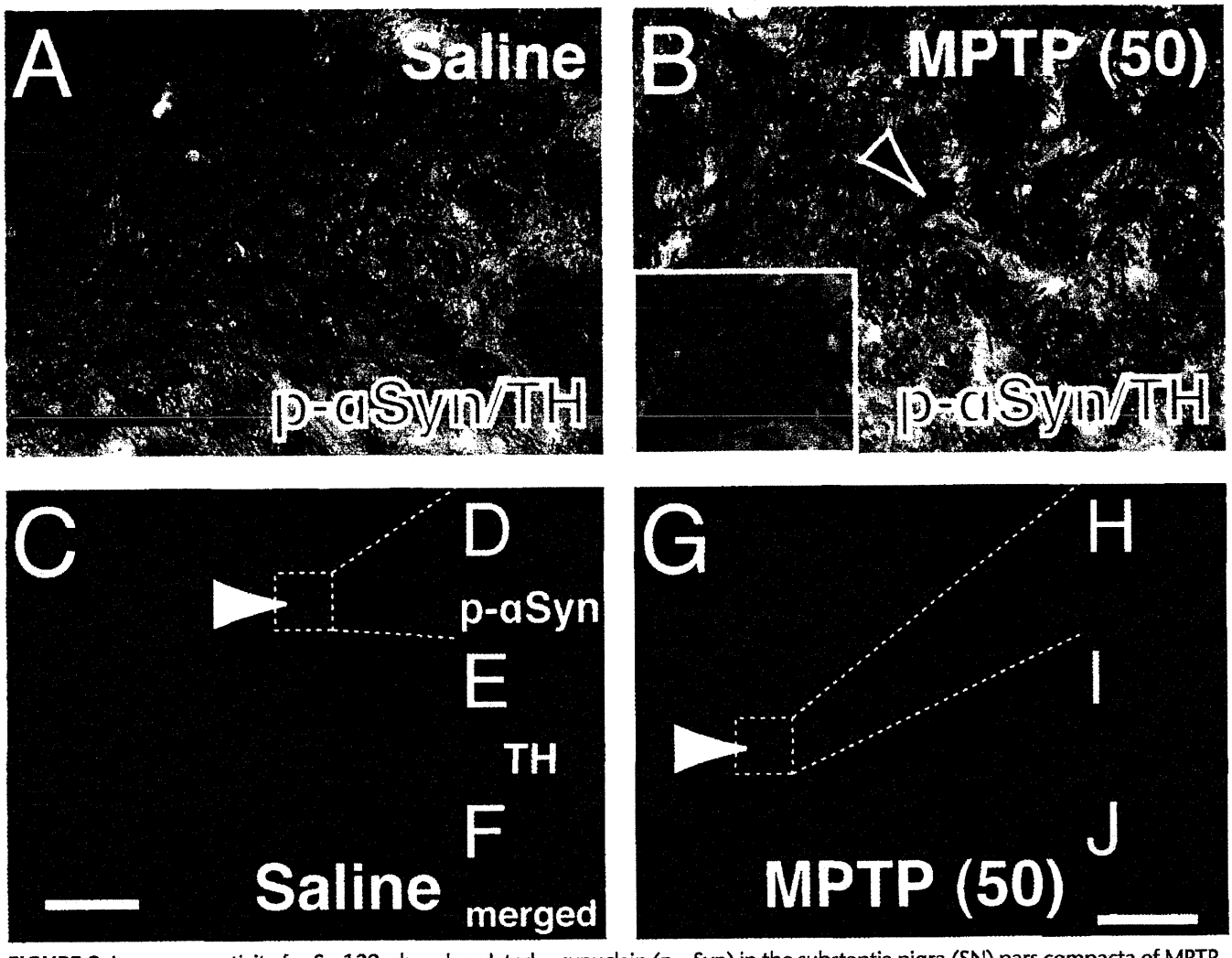

FIGURE 2. Immunoreactivity for Ser129-phosphorylated α-synuclein (p-αSyn) in the substantia nigra (SN) pars compacta of MPTP-minipump mice. **(A, B)** SN sections of saline- **(A)** or MPTP-minipump mice (50 mg/kg per day, MPTP [50]) **(B)** were coimmunostained for the p-αSyn (dark brown/purple) and tyrosine hydroxylase (TH) (brown). p-αSyn–positive cells (arrowhead, enlarged in **[B]** inset) were found in the SN of MPTP-minipump mice. **(C–J)** SN sections of saline- **(C–F)** and MPTP-minipump mice **(G–J)** coimmunostained for the p-αSyn (**C, D, F, G, H, J**, green) and TH (**C, E–G, I, J**, red), merged with anti–p-αSyn in (**C, F, G, J**, yellow) and visualized by fluorescence. Boxed areas in **(C)** and **(G)** are enlarged in **(D–F)** and **(H–J)**, respectively. Scale bars = **(A)** 50 μm (applicable to **B**); **(C)** 50 μm (applicable to **G**); **(J)** 10 μm (applicable to **D–F, H–J**).

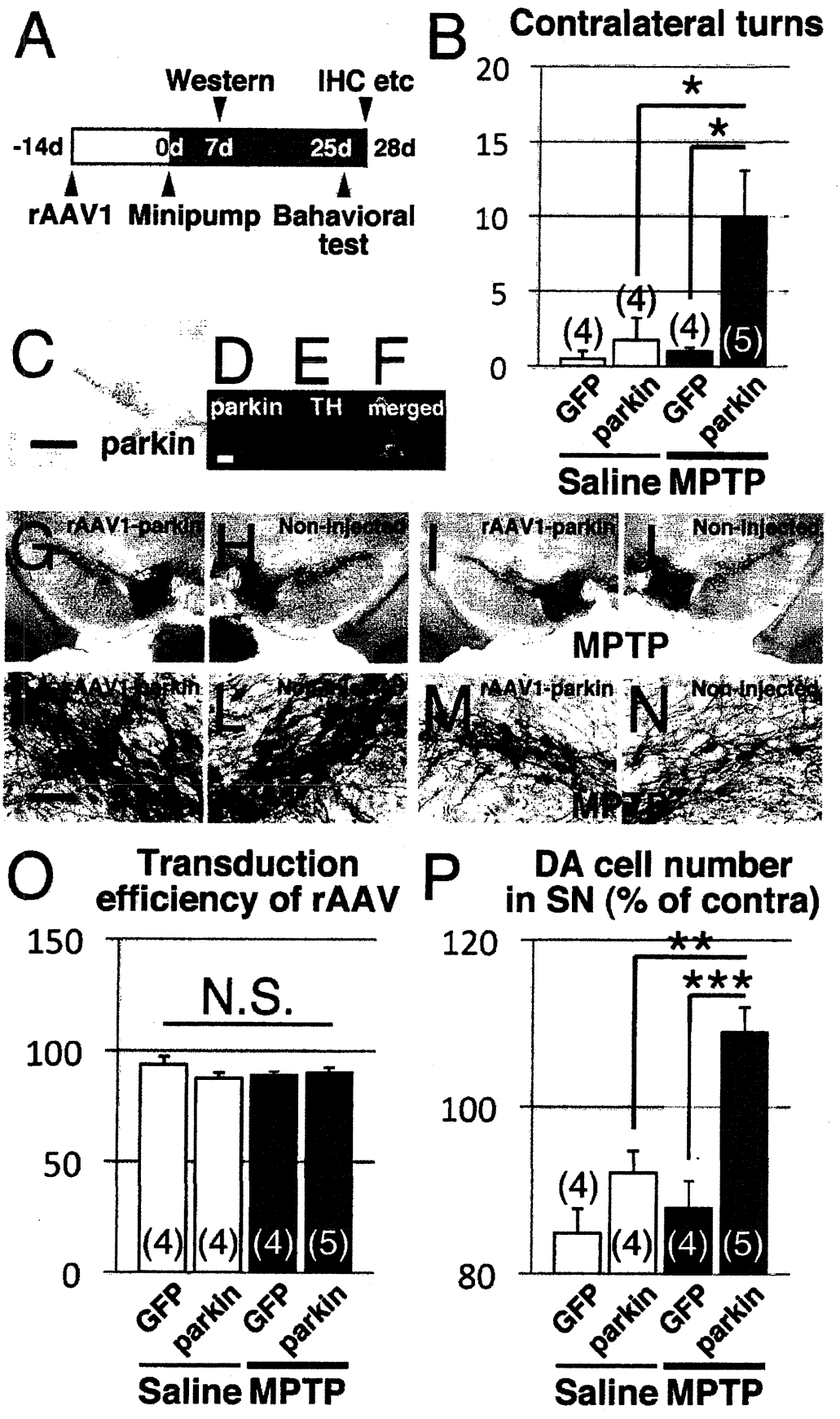

anti-mouse or rabbit IgG secondary antibody (1:500), followed by avidin-biotin-peroxidase complex (ABC Elite) (both from Vector Laboratories, Inc) for 1 hour. Then the sections were reacted in 0.05 mol/L Tris-HCl buffer (pH 7.6) containing 0.04% diaminobenzidine and 0.002% H_2O_2 with (dark brown/purple color) or without (brown color) 0.04% nickel chloride. Images were captured using a light microscope (ACT-1; Nikon Corp, Tokyo, Japan).

Western Blotting

Ventral midbrain tissues were sonicated in chilled CelLytic-MT mammalian tissue lysis/extraction reagent (Sigma) mixed with protease inhibitor cocktail set I (Calbiochem) and phosphatase inhibitor cocktail set V (Calbiochem). The protein concentration in the lysate was determined using BCA protein assay kit (Pierce, Rockford, IL). Each protein sample (10 μg) was resolved by SDS-PAGE by means of Compact-PAGE-twin (ATTO Corp, Tokyo, Japan) and then electrotransferred to Clear Blot Membrane-P (ATTO Corp) using powered BLOTmini (ATTO Corp). The membrane was washed in PBS, incubated for 1 hour in a PBS medium containing 50% ChemiBLOCKER (Millipore Corp) and 0.05% Tween-20, and then incubated for 24 hours with primary antibody in the same fresh medium. Subsequently, the membrane was incubated for 2 hours in fresh medium containing horseradish peroxidase–linked anti-mouse or rabbit IgG secondary antibody (1:10000; GE Healthcare Bio-Sciences, Uppsala, Sweden), followed by development of chemiluminescence using Amersham ECL Plus Western Blotting Detection System (GE Healthcare Bio-Sciences). The image was captured using LAS-3000 (Fujifilm, Tokyo, Japan) and quantified by Image Gauge software. Samples that showed intense protein expression of hrGFP or parkin were used for the subsequent investigations (Table).

Cell Counts

Every eighth 20-μm-thick serial section of the brain was immunostained for parkin (for mice injected with rAAV1-parkin) (Figure, Supplemental Digital Content 1, parts C–J, http://links.lww.com/NEN/A252) or hrGFP (for mice injected with rAAV1-hrGFP). Coimmunostaining for parkin or hrGFP and TH was also performed (Figure, Supplemental Digital Content 1, parts K-M, http://links.lww.com/NEN/A252). Mice that exhibited foreign protein expression in most DA cells in more than ~80% of the area of the entire rostrocaudal region of the SNpc were used for the subsequent investigations (Table). The rostrocaudal area of the SNpc immunopositive for foreign protein was determined in each mouse and used for DA cell counting and phosphorylated αSyn (p-αSyn)–positive cell counting. In every fourth serial section, the numbers of TH- and Nissl-double-positive cells in the SNpc were counted both in the rAAV1-injected and noninjected sides using a stereological method and in a blind manner, as previously reported (35, 38). In brief, SNpc cells with nuclei optimally visible by TH immunostaining and with nuclei, cytoplasm, and nucleoli prominently stained by Nissl staining were counted. To avoid

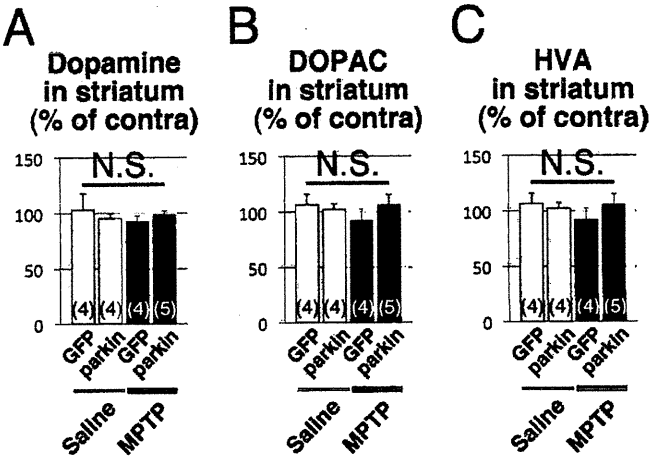

FIGURE 4. Effect of recombinant adeno-associated viral (rAAV1) vector-parkin delivery on striatal levels of dopamine and its metabolites. **(A–C)** The striatal levels of dopamine **(A)**, 2-(3,4-dihydroxyphenyl)acetic acid (DOPAC) **(B)**, and homovanillic acid (HVA) **(C)** in rAAV1-humanized recombinant green fluorescent protein (hrGFP)–injected (denoted as GFP) and the rAAV1-parkin–injected (parkin) saline- (Saline) and MPTP-minipump mice (MPTP). There were no effects on amounts of these compounds. Numbers of analyzed mice in each group are indicated within the bars. Data are expressed as percentage of the contralateral side (% of contra). N.S., not significant (1-way analysis of variance).

FIGURE 3. Recombinant adeno-associated viral (rAAV1) vector-parkin–mediated prevention of behavioral deficit and dopaminergic (DA) cell loss in MPTP-minipump mice. **(A)** Time schedule for gene delivery experiment with rAAV1-parkin. At day 14 after intranigral injection of rAAV1 vector, Alzet osmotic minipumps were implanted i.p. to deliver saline or MPTP at a dose of 50 mg/kg per day for 7 (Western blotting) or 28 days (immunohistochemistry and dopamine measurement). Apomorphine-induced behavioral change was analyzed at day 25 after implantation. **(B)** Apomorphine-induced contralateral turns were counted in rAAV1-humanized recombinant green fluorescent protein (hrGFP)-injected (GFP) or rAAV1-parkin–injected (parkin) saline- (Saline) or MPTP-minipump mice. There was a significant increase in the number of contralateral turns in rAAV1-parkin/MPTP mice. **(C–F)** Substantia nigra (SN) sections of rAAV1-parkin/MPTP mice immunostained for parkin (**C**, brown, **D**, green), and tyrosine hydroxylase (TH) (**E**, red, merged with anti-parkin in **F**, yellow). **(G–N)** Representative photomicrographs of TH- and Nissl-double-positive cells in the ipsilateral (rAAV1-parkin, **G, I, K, M**), and contralateral (noninjected) sides of the SN pars compacta **(H, J, L, N)**, in saline- **(G, H, K, L)** or MPTP-minipump mice **(I, J, M, N)**. **(O)** Transduction efficiencies of the rAAV1 vectors, expressed as percent of the entire rostrocaudal region of the SN. There were no significant differences among the groups. **(P)** Counts of DA cell bodies in the SNpc. Data are expressed as percentage of the contralateral side (% of contra); that is, the cell number in the rAAV1-injected side over that in the noninjected side. rAAV1-parkin ameliorated MPTP-induced DA cell loss. Numbers of mice in each group are indicated within the bars. Data are mean ± SEM. *, $p < 0.05$; **, $p < 0.01$; ***, $p < 0.001$; and N.S., not significant (1-way analysis of variance followed by Tukey-Kramer post hoc test). Scale bars = **(C)** 500 μm (applicable to **G–J**); **(D)** 10 μm (applicable to **D–F**); **(K)** 50 μm (applicable to **K–N**).

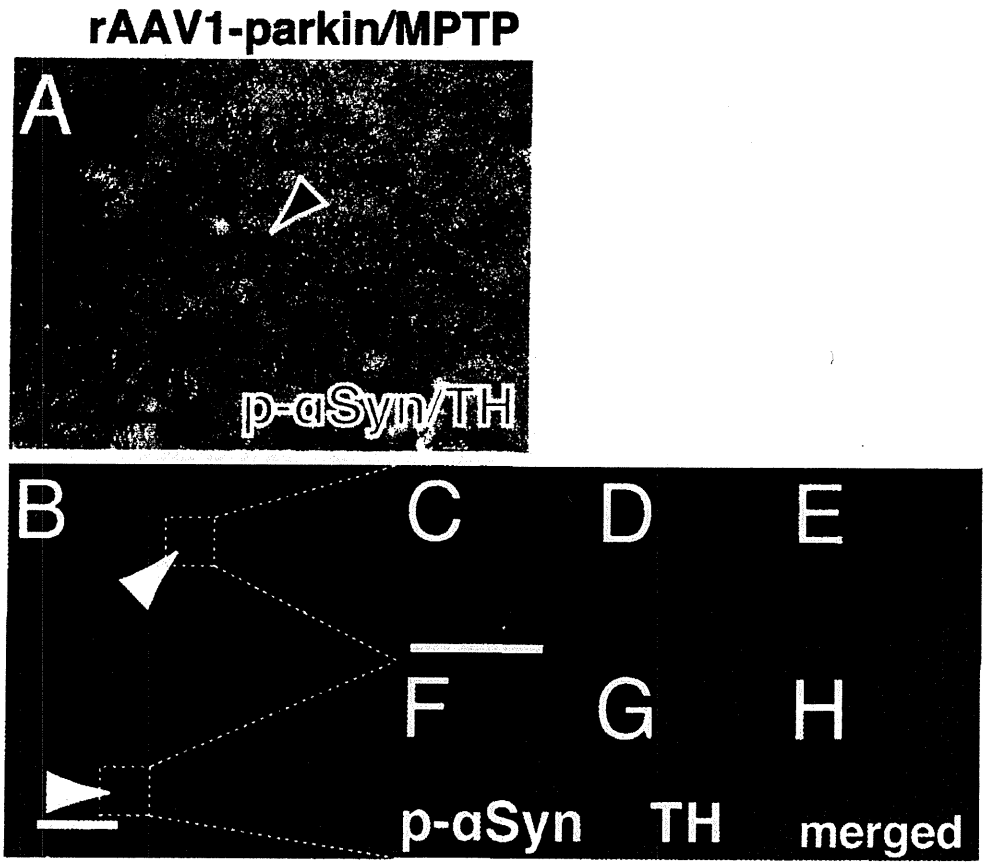

I

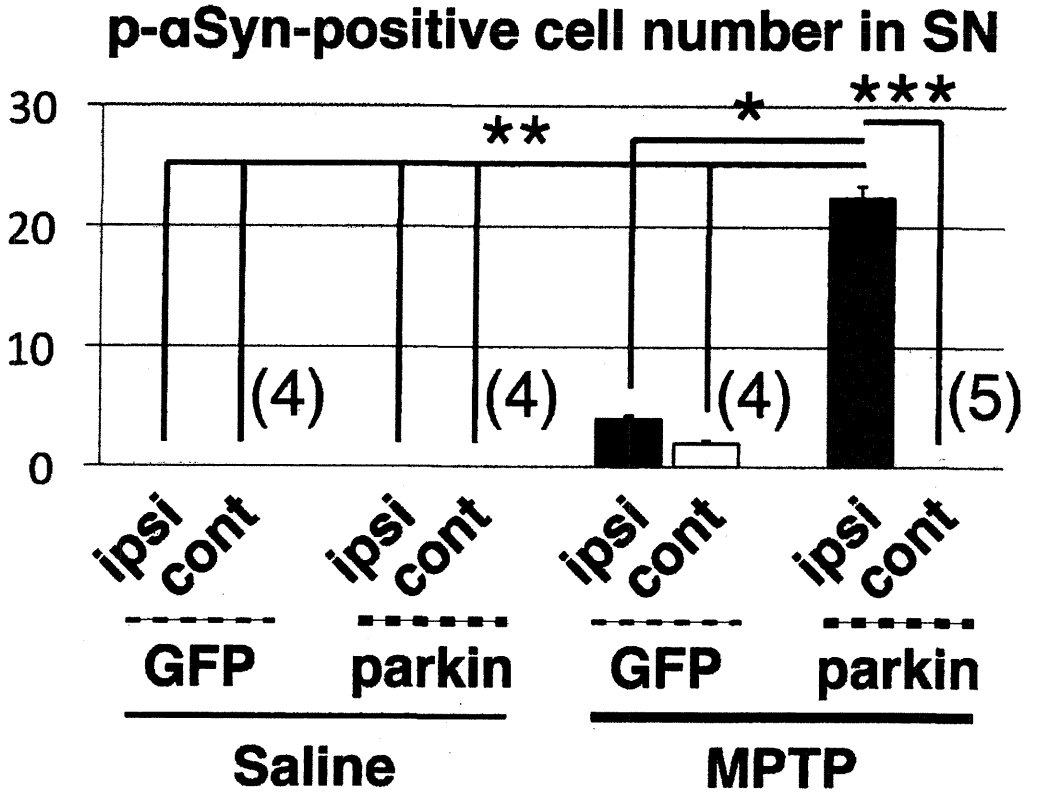

double counting of neurons with unusual shapes, TH- and Nissl-double-positive cells were counted only when their nuclei and nucleoli were optimally visualized. Data were expressed as percentage of the contralateral side, that is, the cell number in the rAAV1-injected side over that in the noninjected side. The numbers of the p-αSyn–positive cells visualized by diaminobenzidine with nickel chloride were counted in every eighth serial section of the SN.

Determination of the Striatal Levels of Dopamine and its Metabolites by High-Performance Liquid Chromatography

Frozen striatal tissues were sonicated in chilled 0.1 mol/L perchloric acid. The samples were centrifuged (20,000 × *g* for 10 minutes at 4°C), and the resulting supernatants were used for the measurement of dopamine, 2-(3,4-dihydroxyphenyl)-acetic acid (DOPAC), and homovanillic acid (HVA) concentrations. The high-performance liquid chromatography (HPLC) system equipped with an 8-electrode coulometric electrochemical detection system (ESA-400; ESA, Inc, Chelmsford, MA) and a reverse-phase C18 column (150 × 4.6 mm; ODS-100s; Tosoh, Tokyo, Japan) was used. The concentrations of dopamine, DOPAC, and HVA were determined in nanomoles per gram of tissue.

Determination of the Striatal Level of 1-Methyl-4-Phenylpyridinium (MPP^+) by HPLC

Mice were killed 24 hours after minipump implantation. Striatal tissues were sonicated in chilled 0.1 mol/L perchloric acid containing 0.1 mmol/L EDTA and an internal standard, 10 mmol/L 4-phenylpyridine (Sigma-Aldrich Corp). The samples were centrifuged (20,000 × *g* for 10 minutes at 4°C), and the resulting supernatants were used for MPP^+ concentration measurement (nmol/g of tissue). The HPLC system AKTA explorer (GE Healthcare Bio-Sciences) equipped with a reverse-phase C18 column (150 × 4.6 mm; ODS-100s; Tosoh) was used.

Statistical Analysis

All data are expressed as mean ± SEM. Two-tailed Student *t*-test (for 2 groups) and 1-way analysis of variance (ANOVA), followed by Tukey-Kramer post hoc test (for ≥3 groups) were applied. A p value less than 0.05 denoted statistically significant differences.

RESULTS

Generation of a High-Dose and Long-Term MPTP Infusion Model Using Alzet Osmotic Minipumps

The 50- and 100-mg/kg-per-day MPTP-minipump mice had 61.3% ± 6.3% ($p = 0.003262$; $df = 9$; 1-way ANOVA followed by Tukey-Kramer post hoc test) and 46.1% ± 5.6% ($p = 0.0006822$) of DA cell bodies in the SNpc found in the saline controls (Figs. 1A–G); they had 48.1% ± 5.1% ($p = 6.646 \times 10^{-6}$; $df = 22$) and 31.2% ± 5.1% ($p = 9.808 \times 10^{-8}$) of dopamine in the striatum found in the saline group, respectively (Fig. 1H). Dopamine metabolites, DOPAC and HVA, were also decreased (Figs. 1I, J). Levels of striatal MPP^+ (the active metabolite of MPTP) were 4.23 ± 1.46 nmol/g tissue ($p < 0.05$ vs the saline control group) and 7.05 ± 0.64 nmol/g tissue ($p < 0.001$ vs control) for the 50- and 100-mg/kg-per-day regimens, respectively ($p < 0.05$ and $p < 0.001$, by 1-way ANOVA followed by Tukey-Kramer post hoc test). Despite the loss of nigrostriatal DA neurons 28 days after the implantation, behavioral changes were not evident by rotarod test (even in the 100-mg/kg-per-day MPTP group) at 25 days after implantation of minipumps (latency time to fall: 198.3 ± 26.0 seconds in the saline group and 229.7 ± 17.2 seconds in the 100-mg/kg-per-day MPTP group; $p = 0.3461$).

Immunoreactivity for the Ser129-Phosphorylated αSyn in the SN of MPTP-Minipump Mice

Fornai et al (39) previously observed electron-dense and fibrillar neuronal inclusions containing αSyn in the SN of MPTP-minipump model mice. One of the critical pathogenic modifications of αSyn is the phosphorylation at Ser129 residue (40); therefore, we examined Ser129-p-αSyn immunoreactivity in the SN of our MPTP-minipump mice. In preliminary studies, the anti-p-αSyn antibody was evaluated using nigral sections of mice that had received a stereotaxic intranigral injection of rAAV1 vector encoding human αSyn (Figure, Supplemental Digital Content 2, http://links.lww.com/NEN/A253). The antibody reacted specifically with DA cell bodies in the ipsilateral side of the SN (Figure, Supplemental Digital Content 2, parts B-E, I-K, http://links.lww.com/NEN/A253) in which human αSyn is overexpressed (Figure, Supplemental Digital Content 2, parts 2 A, D, J, http://links.lww.com/NEN/A253). We found a small number of p-αSyn–immunopositive cells in the SN of MPTP-minipump (50 mg/kg per day) mice (Figs. 2B, G–J; see also Fig. 5I). These cells were not seen in saline-minipump mice (Figs. 2A, C–F; also see Fig. 5I).

Amelioration of Nigral DA Cell Loss by rAAV1-Mediated Parkin Overexpression in MPTP-Minipump Mice

We next investigated the effect of rAAV1-mediated overexpression of parkin on the survival of DA neurons in MPTP-minipump mice. High-titer rAAV1-parkin or rAAV1-hrGFP was injected unilaterally into the SN of C57BL/6 mice.

FIGURE 5. Ser129-phosphorylated αSyn (p-αSyn) immunoreactivity in the substantia nigra (SN) pars compacta of MPTP-minipump mice injected with recombinant adeno-associated viral (rAAV1) vector-parkin. **(A)** SN sections of rAAV1-parkin/MPTP mice coimmunostained for the p-αSyn (dark brown/purple) and tyrosine hydroxylase (TH) (brown) and visualized using diaminobenzidine. A p-αSyn–positive cell is indicated by arrowhead. **(B–H)** SN sections of rAAV1-parkin/MPTP mice coimmunostained for p-αSyn (**B, C, E, F, H**, green) and TH (**B, D, E, G, H**, red), merged with anti-p-αSyn (**B, E, H**, yellow), and visualized by fluorescence. Boxed areas in **(B)** are enlarged in (**C–E** and **F–H**). **(I)** Counts of p-αSyn–positive cells in the SN, visualized by diaminobenzidine. Injection of rAAV1-parkin significantly increased the p-αSyn–positive cells in MPTP-minipump mice. Numbers of analyzed mice in each group are indicated. Data are mean ± SEM. *, $p < 0.05$; **, $p < 0.01$; and ***, $p < 0.001$ (1-way analysis of variance followed by Tukey-Kramer post hoc test). Scale bars = **(A)** 50 μm; **(B)** 50 μm; **(C)** 10 μm (applicable to **(C–H)**).

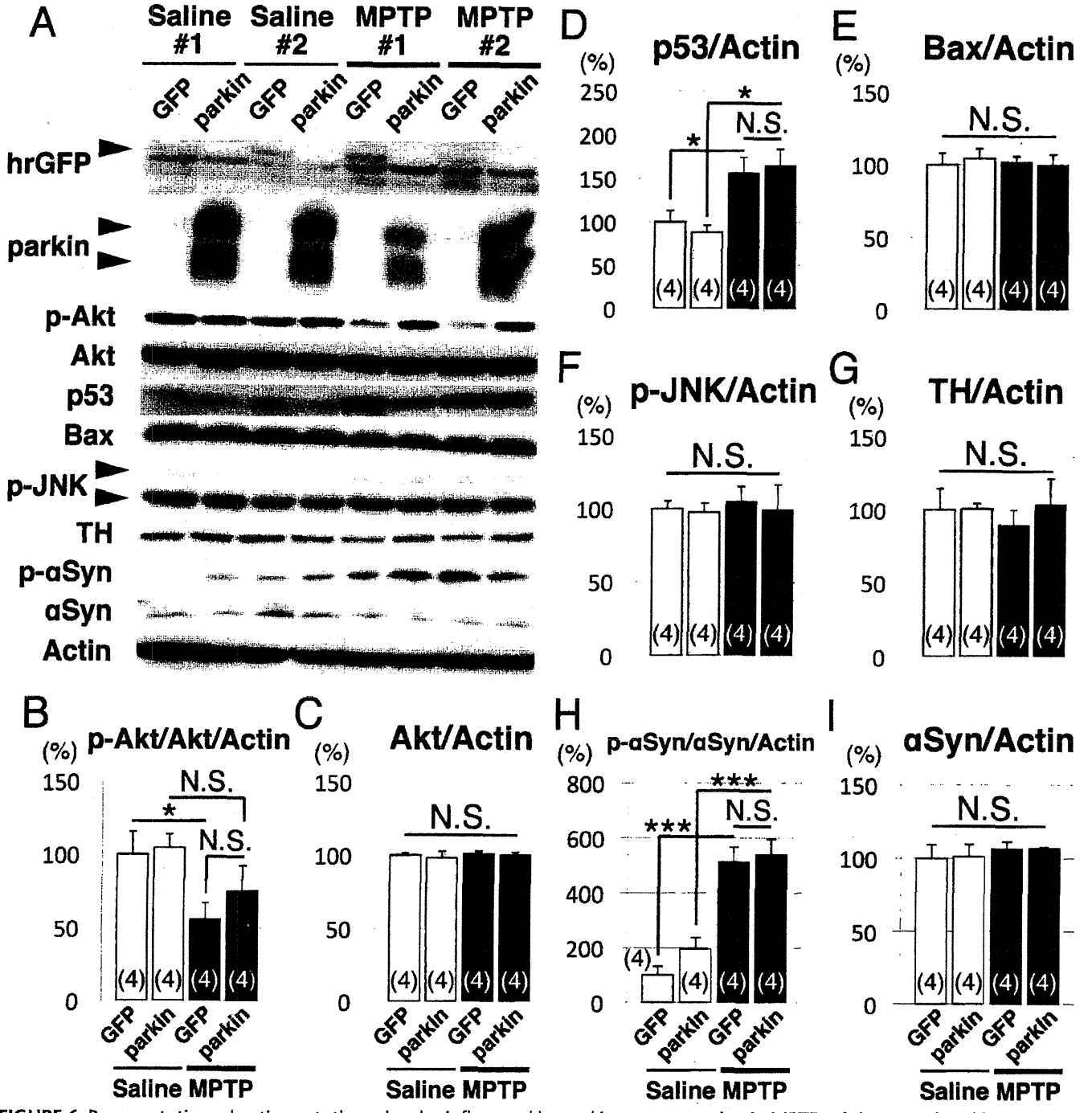

FIGURE 6. Proapoptotic and antiapoptotic molecules influenced by parkin overexpression in MPTP-minipump mice. **(A)** Western blotting was performed using midbrain tissues of mice killed 7 days after minipump implantation. Phosphorylated Akt (p-Akt) was reduced in the rAAV1-humanized recombinant green fluorescent protein (hrGFP)–injected side (GFP) but not in the rAAV1-parkin–injected side (parkin) of MPTP-minipump mice. **(B–G)** Data are presented as percentage of control (GFP/saline group) for p-Akt/Akt/Actin **(B)**, Akt/Actin **(C)**, p53/Actin **(D)**, Bax/Actin **(E)**, the phosphorylated JNK (p-JNK)/Actin **(F)**, tyrosine hydroxylase (TH)/Actin **(G)**, p-αSyn/αSyn/Actin **(H)**, and αSyn/Actin **(I)**. Reduction of p-Akt was significant in the rAAV1-hrGFP/MPTP group but not in the rAAV1-parkin/MPTP group. Total protein amount of Akt was unchanged. The protein levels of p53 and p-αSyn were significantly increased in the MPTP groups, and there were nonsignificant differences between the rAAV1-hrGFP/MPTP and rAAV1-parkin/MPTP groups. Numbers of mice analyzed in each group are indicated within the bars. Data are mean ± SEM. *, $p < 0.05$; and N.S., not significant (1-way analysis of variance followed by Tukey-Kramer post hoc test).

At 14 days after injection of the rAAV1 vectors, mice were implanted with minipumps to deliver MPTP at dose of 50 mg/kg per day (Fig. 3A; Table). Mice were examined for an apomorphine-induced rotation behavior 25 days after the treatment with MPTP. The injection of rAAV1-parkin resulted in increased contralateral turns in MPTP-minipump mice compared with rAAV1-parkin/saline ($p = 0.04633$; $df = 16$) and rAAV1-hrGFP/MPTP mice ($p = 0.02843$) (Fig. 3B). This suggests functional preservation of the nigrostriatal pathways provided by parkin delivery. Immunohistochemistry revealed overexpression of parkin in TH-positive DA cells in the SNpc (Figs. 3C–F; Figure, Supplemental Digital Content 1, parts 1C–M, http://links.lww.com/NEN/A252). Next, we counted TH- and Nissl-double-positive cells in the SNpc of these mice. As shown in Figures 3G to N and P, the injection of rAAV1 vector itself (i.e. in saline-treated groups) caused a minor decrease of DA cell number (15.1% ± 2.9% decrease in the rAAV1-hrGFP–injected mice and 7.9% ± 2.6% decrease in the rAAV1-parkin–injected mice). Importantly, rAAV1-parkin delivery promoted the survival of DA cell bodies in MPTP-minipump mice (109.0% ± 2.9% relative to the contralateral noninjected side) compared with parkin-overexpressed saline-minipump mice ($p = 0.005143$; $df = 16$) and hrGFP-overexpressed MPTP-minipump mice (88.0% ± 3.2%; $p = 0.0008401$) (Fig. 3P). The transduction efficiency of the rAAV1 vectors (i.e. the area immunopositive for parkin or hrGFP over the entire rostrocaudal area of the SNpc) varied from 87.5% ± 2.6% to 93.75% ± 3.6%, which had no statistical difference among the groups (Fig. 3O; Figure, Supplemental Digital Content 1, parts 1C-M, http://links.lww.com/NEN/A252). On the other hand, the striatal level of dopamine was not preserved with the injection of rAAV1-parkin, the same as with rAAV1-hrGFP (Fig. 4A). There was no influence on the striatal levels of dopamine metabolites, DOPAC and HVA, in these mice (Figs. 4B, C).

Accumulation of Ser129-Phosphorylated αSyn Promoted by Parkin Overexpression

There were increased numbers of p-αSyn–positive cell bodies in the rAAV1-parkin–injected side of the SN in MPTP-minipump mice (Figs. 5A–I). Thus, parkin delivery enhanced accumulation of the p-αSyn in DA cells in MPTP-minipump mice.

Alleviation of MPTP-Induced Inactivation of Akt by Parkin Delivery

On the basis of our previous report that showed upregulation of Bax 6 to 8 days after the first treatment with MPTP (30 mg/kg per day for 5 consecutive days) (41), we performed Western analyses at 7 days after minipump implantation (Fig. 3A). As shown in Figure 6, TH protein was slightly but nonsignificantly reduced by MPTP treatment and parkin counteracted the effect (Figs. 6A, G). There were no significant influences on the protein amounts of proapoptotic Bax (Figs. 6A, E) and the phosphorylated active form of JNK (Figs. 6A, F) in this model. The level of p53 was increased significantly in MPTP-minipump mice but had no significant difference between the rAAV1-hrGFP and rAAV1-parkin groups (Figs. 6A, D). Importantly, phosphorylated Akt, an active form of a prosurvival kinase Akt, was reduced in the rAAV1-hrGFP–injected hemisphere of MPTP-minipump mice ($p = 0.02829$; $df = 15$; compared with rAAV1-hrGFP/saline); the decrease was alleviated by rAAV1-parkin ($p = 0.8434$; compared with rAAV1-parkin/saline) (Figs. 6A, B). The level of total Akt protein was not changed by MPTP (Figs. 6A, C), indicating that parkin diminished the MPTP-induced dephosphorylation of p-Akt. p-αSyn was increased in response to MPTP ($p = 0.0001902$; $df = 15$; compared between rAAV1-hrGFP/saline and rAAV1-hrGFP/MPTP groups; and $p = 0.0009918$; compared between rAAV1-parkin/saline and rAAV1-parkin/MPTP groups), although there was no difference between the hrGFP and parkin groups at this time point ($p = 0.9780$; compared between rAAV1-hrGFP/MPTP and rAAV1-parkin/MPTP groups) (Figs. 6A, H). A similar result was obtained with another anti–p-αSyn antibody (clone pSyn#64; Wako; Figure, Supplemental Digital Content 3, part A, http://links.lww.com/NEN/A254). The total amount of αSyn protein was not changed by MPTP (Figs. 6A, I).

Effects of Parkin Overexpression on Mitochondrial Alterations

Finally, we addressed the effect of intranigral parkin delivery on the protein levels of PINK1 and a mitochondrial protein marker Tom20. Western blotting analysis demonstrated that both MPTP treatment and parkin expression rendered PINK1 to increase slightly but nonsignificantly (Figure, Supplemental Digital Content 3, parts A, B, http://links.lww.com/NEN/A254). The protein amounts of Tom20 and DJ-1 were not changed at this time point (Figure, Supplemental Digital Content 3, parts A, C, D, http://links.lww.com/NEN/A254). At day 28 after implantation of the minipumps, there was increased immunoreactivity for Tom20 in the SNpc of MPTP-minipump mice (Figure, Supplemental Digital Content 3, parts E-J, K-Z′, http://links.lww.com/NEN/A254); however, this phenomenon was not influenced by overexpression of parkin (Figure, Supplemental Digital Content 3, parts K-Z′, http://links.lww.com/NEN/A254). The overexpressed parkin was found scarcely colocalized with the mitochondrial Tom20 (Figure, Supplemental Digital Content 3, parts L-N′, P-R′, T-V′, and X-Z′, http://links.lww.com/NEN/A254).

DISCUSSION

In the present study, we generated a modified high-dose and long-term mouse model of PD using Alzet osmotic minipump administration of MPTP. In our preliminary experiments, we tried to produce an MPTP-minipump model according to the regimen of Fornai et al (39) but were unsuccessful. Alvarez-Fischer et al (42) recently demonstrated that an Alzet minipump-mediated infusion of MPTP alone (40 mg/kg per day for 3 weeks) caused only a transient depletion of the striatal dopamine and no DA cell loss in the SN. They further indicated that minipump-mediated infusion of MPTP (40–80 mg/kg per day for 2–4 weeks) in combination with the uricosuric agent probenecid caused moderate degeneration of DA neurons (42). We did not attempt to

inhibit renal excretion and/or brain efflux clearance of MPTP/MPP$^+$ but could generate a novel MPTP-minipump model by simply increasing the dose of MPTP to 50 and 100 mg/kg per day.

In this long-term environmental model of PD, we first evaluated the therapeutic effect of parkin. The rAAV vector was chosen because of its ability for long-term stable gene expression in postmitotic neurons with low accompanying cytotoxicities (43, 44). These properties are preferable for recent clinical trials to treat neurodegenerative disorders including PD (44, 45). Paterna et al (26) reported that rAAV vector–mediated transduction of parkin protected DA neurons of mice that were treated transiently with low dose of MPTP (20 mg/kg per day for 4 days). Our present data are in line with those results and indicate further that *parkin* gene therapy might be effective in a more severe and continuous condition causing PD. In 6-hydroxydopamine–lesioned rats, Vercammen et al (25) reported that lentiviral vector-parkin delivery resulted in a significant preservation of DA cell bodies and nerve terminals with corresponding behavioral improvement; by contrast, another group demonstrated that rAAV-parkin delivery ameliorated motor deficits but had no protection on the striatal DA innervation and nigral TH-positive neurons (46). In the present study, the MPTP-induced decrease of striatal dopamine was not prevented by rAAV1-parkin, whereas motor deficits and DA cell loss were ameliorated. We speculate that this discrepancy might be a result of an enhanced dopamine release of the surviving DA neurons that overexpress parkin (46), in consideration with an impaired dopamine release in parkin knockout mice (18).

We observed more the p-αSyn–immunopositive cells in the parkin-overexpressed SN of MPTP-minipump mice. There have been conflicting reports about the neurotoxicity of the p-αSyn in αSyn overexpression PD models; alteration of Ser129 to nonphosphorylated Ala or a phospho-mimetic Asp resulted in enhanced, eliminated, or unchanged the neurotoxicity of αSyn (47–51). Our present data imply that parkin delivery promoted DA neuronal survival in part by increasing the accumulation of the p-αSyn. This is consistent with the report by Gorbatyuk et al (48), who demonstrated that rAAV-mediated overexpression of αSyn Ser129Asp (which seemed to form punctate inclusions) caused no pathologic change in the SN. It has been speculated that parkin promoted accumulation of αSyn through catalyzing a nonclassic polyubiquitination of modified αSyn and/or αSyn-interacting proteins (13).

We found that MPTP-induced reduction of the phosphorylated active form of Akt was prevented by parkin overexpression. Recent work indicated that parkin potentiates epidermal growth factor (EGF)–induced activation of Akt signaling through interfering with Eps15, a negative regulator of the EGF/EGF receptor pathway (52). It is known that rAAV vector–mediated transduction of constitutively active form of Akt can provide DA neuroprotection in 6-hydroxydopamine mice (53). Moreover, Aleyasin et al (54) recently reported that DJ-1 (the loss-of-function mutations of which cause another form of recessively inherited PD) is necessary for Akt-mediated neuronal protection against MPTP. In agreement with these reports, our results suggest that maintenance of Akt signaling by parkin is important for the promotion of DA neuronal survival. On the other hand, da Costa et al (55) demonstrated that parkin elicits ubiquitin ligase-independent transcriptional repression of *p53* gene. In our present experiments, however, we did not find that ectopic parkin counteracted against the MPTP-induced upregulation of p53.

Parkin acts in concert with PINK1 in mitochondrial quality control (29–33). Overexpressed parkin interacts directly with and stabilizes PINK1 (56). Mitochondrial impairment also stabilizes PINK1, and recruitment of parkin to the damaged mitochondria is dependent on PINK1 in mitophagy (30, 31, 33). In the present study, the virally expressed parkin seemed not to affect the clearance of mitochondria that were damaged with MPTP treatment. These results suggest that a long-term insult makes it difficult for parkin to be effective in eliminating potentially harmful accumulated mitochondria.

In conclusion, the present study lends support to the hypothesis that the rAAV vector–mediated *parkin* gene therapy may have clinical benefits for advanced patients with idiopathic PD (16, 45, 57) and provides a new insight into the neuroprotective actions of multifunctional parkin in animal PD models.

ACKNOWLEDGMENT

The authors thank Hideki Shimura, MD, PhD, Department of Neurology, Juntendo University Urayasu Hospital, for his excellent advice.

REFERENCES

1. Farrer MJ. Genetics of Parkinson disease: Paradigm shifts and future prospects. Nat Rev Genet 2006;7:306–18
2. Shults CW. Lewy bodies. Proc Natl Acad Sci U S A 2006;103:1661–68
3. Dauer W, Przedborski S. Parkinson's disease: Mechanisms and models. Neuron 2003;39:889–909
4. Kitada T, Asakawa S, Hattori N, et al. Mutations in the *parkin* gene cause autosomal recessive juvenile parkinsonism. Nature 1998;392:605–8
5. Shimura H, Hattori N, Kubo S, et al. Familial Parkinson disease gene product, *parkin*, is a ubiquitin-protein ligase. Nat Genet 2000;25:302–5
6. Takahashi H, Ohama E, Suzuki S, et al. Familial juvenile parkinsonism: Clinical and pathologic study in a family. Neurology 1994;44:437–41
7. Mori H, Kondo T, Yokochi M. Pathologic and biochemical studies of juvenile parkinsonism linked to chromosome 6q. Neurology 1998;51: 890–92
8. Hayashi S, Wakabayashi K, Ishikawa A, et al. An autopsy case of autosomal-recessive juvenile parkinsonism with a homozygous exon 4 deletion in the *parkin* gene. Mov Disord 2000;15:884–88
9. van de Warrenburg BP, Lammens M, Lucking CB, et al. Clinical and pathologic abnormalities in a family with parkinsonism and *parkin* gene mutations. Neurology 2001;56:555–57
10. Savitt JM, Dawson VL, Dawson TM. Diagnosis and treatment of Parkinson disease: Molecules to medicine. J Clin Invest 2006;116:1744–54
11. Moore DJ. Parkin: A multifaceted ubiquitin ligase. Biochem Soc Trans 2006;34:749–53
12. Lim KL, Chew KC, Tan JM, et al. Parkin mediates nonclassical, proteasomal-independent ubiquitination of synphilin-1: Implications for Lewy body formation. J Neurosci 2005;25:2002–9
13. Lim KL, Dawson VL, Dawson TM. Parkin-mediated lysine 63–linked polyubiquitination: A link to protein inclusions formation in Parkinson's and other conformational diseases? Neurobiol Aging 2006;27:524–29
14. Doss-Pepe EW, Chen L, Madura K. alpha-Synuclein and *parkin* contribute to the assembly of ubiquitin lysine 63–linked multiubiquitin chains. J Biol Chem 2005;280:16619–24

15. Mukhopadhyay D, Riezman H. Proteasome-independent functions of ubiquitin in endocytosis and signaling. Science 2007;315:201–5
16. Yasuda T, Mochizuki H. The regulatory role of alpha-synuclein and *parkin* in neuronal cell apoptosis: Possible implications for the pathogenesis of Parkinson's disease. Apoptosis 2010;15:1312–21
17. Palacino JJ, Sagi D, Goldberg MS, et al. Mitochondrial dysfunction and oxidative damage in *parkin*-deficient mice. J Biol Chem 2004;279: 18614–22
18. Kitada T, Pisani A, Karouani M, et al. Impaired dopamine release and synaptic plasticity in the striatum of *parkin*−/− mice. J Neurochem 2009; 110:613–21
19. Frank-Cannon TC, Tran T, Ruhn KA, et al. Parkin deficiency increases vulnerability to inflammation-related nigral degeneration. J Neurosci 2008; 28:10825–34
20. Chung KK, Thomas B, Li X, et al. *S*-nitrosylation of parkin regulates ubiquitination and compromises *parkin*'s protective function. Science 2004;304:1328–31
21. Yao D, Gu Z, Nakamura T, et al. Nitrosative stress linked to sporadic Parkinson's disease: *S*-nitrosylation of parkin regulates its E3 ubiquitin ligase activity. Proc Natl Acad Sci U S A 2004;101:10810–14
22. LaVoie MJ, Ostaszewski BL, Weihofen A, et al. Dopamine covalently modifies and functionally inactivates parkin. Nat Med 2005;11:1214–21
23. Ng CH, Mok SZ, Koh C, et al. Parkin protects against LRRK2 G2019S mutant-induced dopaminergic neurodegeneration in *Drosophila*. J Neurosci 2009;29:11257–62
24. Yang Y, Gehrke S, Imai Y, et al. Mitochondrial pathology and muscle and dopaminergic neuron degeneration caused by inactivation of *Drosophila* Pink1 is rescued by Parkin. Proc Natl Acad Sci U S A 2006; 103:10793–98
25. Vercammen L, Van der Perren A, Vaudano E, et al. Parkin protects against neurotoxicity in the 6-hydroxydopamine rat model for Parkinson's disease. Mol Ther 2006;14:716–23
26. Paterna JC, Leng A, Weber E, et al. DJ-1 and Parkin modulate dopamine-dependent behavior and inhibit MPTP-induced nigral dopamine neuron loss in mice. Mol Ther 2007;15:698–704
27. Yamada M, Mizuno Y, Mochizuki H. Parkin gene therapy for alpha-synucleinopathy: A rat model of Parkinson's disease. Hum Gene Ther 2005;16:262–70
28. Yasuda T, Miyachi S, Kitagawa R, et al. Neuronal specificity of alpha-synuclein toxicity and effect of Parkin co-expression in primates. Neuroscience 2007;144:743–53
29. Whitworth AJ, Pallanck LJ. The PINK1/Parkin pathway: A mitochondrial quality control system? J Bioenerg Biomembr 2009;41:499–503
30. Vives-Bauza C, Zhou C, Huang Y, et al. PINK1-dependent recruitment of Parkin to mitochondria in mitophagy. Proc Natl Acad Sci U S A 2010; 107:378–83
31. Narendra DP, Jin SM, Tanaka A, et al. PINK1 is selectively stabilized on impaired mitochondria to activate Parkin. PLoS Biol 2010;8:e1000298
32. Geisler S, Holmstrom KM, Skujat D, et al. PINK1/Parkin-mediated mitophagy is dependent on VDAC1 and p62/SQSTM1. Nat Cell Biol 2010;12:119–31
33. Matsuda N, Sato S, Shiba K, et al. PINK1 stabilized by mitochondrial depolarization recruits Parkin to damaged mitochondria and activates latent Parkin for mitophagy. J Cell Biol 2010;189:211–21
34. Yamada M, Iwatsubo T, Mizuno Y, et al. Overexpression of alpha-synuclein in rat substantia nigra results in loss of dopaminergic neurons, phosphorylation of alpha-synuclein and activation of caspase-9: Resemblance to pathogenetic changes in Parkinson's disease. J Neurochem 2004; 91:451–61
35. Yasuda T, Nihira T, Ren YR, et al. Effects of UCH-L1 on alpha-synuclein over-expression mouse model of Parkinson's disease. J Neurochem 2009; 108:932–44
36. Przedborski S, Jackson-Lewis V, Naini AB, et al. The parkinsonian toxin 1-methyl-4-phenyl-1,2,3,6-tetrahydropyridine (MPTP): A technical review of its utility and safety. J Neurochem 2001;76:1265–74
37. Da Cunha C, Wietzikoski EC, Ferro MM, et al. Hemiparkinsonian rats rotate toward the side with the weaker dopaminergic neurotransmission. Behav Brain Res 2008;189:364–72
38. Furuya T, Hayakawa H, Yamada M, et al. Caspase-11 mediates inflammatory dopaminergic cell death in the 1-methyl-4-phenyl-1,2,3,6-tetrahydropyridine mouse model of Parkinson's disease. J Neurosci 2004; 24:1865–72
39. Fornai F, Schluter OM, Lenzi P, et al. Parkinson-like syndrome induced by continuous MPTP infusion: Convergent roles of the ubiquitin-proteasome system and alpha-synuclein. Proc Natl Acad Sci U S A 2005; 102:3413–18
40. Fujiwara H, Hasegawa M, Dohmae N, et al. alpha-Synuclein is phosphorylated in synucleinopathy lesions. Nat Cell Biol 2002;4:160–64
41. Cao XQ, Arai H, Ren YR, et al. Recombinant human granulocyte colony-stimulating factor protects against MPTP-induced dopaminergic cell death in mice by altering Bcl-2/Bax expression levels. J Neurochem 2006;99:861–67
42. Alvarez-Fischer D, Guerreiro S, Hunot S, et al. Modelling Parkinson-like neurodegeneration via osmotic minipump delivery of MPTP and probenecid. J Neurochem 2008;107:701–11
43. Burger C, Gorbatyuk OS, Velardo MJ, et al. Recombinant AAV viral vectors pseudotyped with viral capsids from serotypes 1, 2, and 5 display differential efficiency and cell tropism after delivery to different regions of the central nervous system. Mol Ther 2004;10:302–17
44. Mandel RJ, Manfredsson FP, Foust KD, et al. Recombinant adeno-associated viral vectors as therapeutic agents to treat neurological disorders. Mol Ther 2006;13:463–83
45. Mochizuki H, Yasuda T, Mouradian MM. Advances in gene therapy for movement disorders. Neurotherapeutics 2008;5:260–69
46. Manfredsson FP, Burger C, Sullivan LF, et al. rAAV-mediated nigral human parkin over-expression partially ameliorates motor deficits via enhanced dopamine neurotransmission in a rat model of Parkinson's disease. Exp Neurol 2007;207:289–301
47. Chen L, Feany MB. alpha-Synuclein phosphorylation controls neurotoxicity and inclusion formation in a *Drosophila* model of Parkinson disease. Nat Neurosci 2005;8:657–63
48. Gorbatyuk OS, Li S, Sullivan LF, et al. The phosphorylation state of Ser-129 in human alpha-synuclein determines neurodegeneration in a rat model of Parkinson disease. Proc Natl Acad Sci U S A 2008;105: 763–68
49. Azeredo da Silveira S, Schneider BL, Cifuentes-Diaz C, et al. Phosphorylation does not prompt, nor prevent, the formation of alpha-synuclein toxic species in a rat model of Parkinson's disease. Hum Mol Genet 2009; 18:872–87
50. Chen L, Periquet M, Wang X, et al. Tyrosine and serine phosphorylation of alpha-synuclein have opposing effects on neurotoxicity and soluble oligomer formation. J Clin Invest 2009;119:3257–65
51. McFarland NR, Fan Z, Xu K, et al. alpha-Synuclein S129 phosphorylation mutants do not alter nigrostriatal toxicity in a rat model of Parkinson disease. J Neuropathol Exp Neurol 2009;68:515–24
52. Fallon L, Belanger CM, Corera AT, et al. A regulated interaction with the UIM protein Eps15 implicates parkin in EGF receptor trafficking and PI(3)K-Akt signalling. Nat Cell Biol 2006;8:834–42
53. Ries V, Henchcliffe C, Kareva T, et al. Oncoprotein Akt/PKB induces trophic effects in murine models of Parkinson's disease. Proc Natl Acad Sci U S A 2006;103:18757–62
54. Aleyasin H, Rousseaux MW, Marcogliese PC, et al. DJ-1 protects the nigrostriatal axis from the neurotoxin MPTP by modulation of the AKT pathway. Proc Natl Acad Sci U S A 2010;107:3186–91
55. da Costa CA, Sunyach C, Giaime E, et al. Transcriptional repression of p53 by parkin and impairment by mutations associated with autosomal recessive juvenile Parkinson's disease. Nat Cell Biol 2009;11:1370–75
56. Shiba K, Arai T, Sato S, et al. Parkin stabilizes PINK1 through direct interaction. Biochem Biophys Res Commun 2009;383:331–35
57. Mochizuki H. Parkin gene therapy. Parkinsonism Relat Disord 2009;15: S43–45

EJN fens EUROPEAN JOURNAL OF NEUROSCIENCE

European Journal of Neuroscience, Vol. 34, pp. 1355–1367, 2011 doi:10.1111/j.1460-9568.2011.07873.x

MOLECULAR AND DEVELOPMENTAL NEUROSCIENCE

Postnatal development of tyrosine hydroxylase mRNA-expressing neurons in mouse neostriatum

Masao Masuda,[1,*] Masami Miura,[1] Ritsuko Inoue,[1] Michiko Imanishi,[2] Sachiko Saino-Saito,[3,†] Masahiko Takada,[2,‡] Kazuto Kobayashi[4] and Toshihiko Aosaki[1]

[1]Neuropathophysiology Research Group, Tokyo Metropolitan Institute of Gerontology, Itabashi, Tokyo, Japan
[2]Department of System Neuroscience, Tokyo Metropolitan Institute for Neuroscience, Fuchu, Tokyo, Japan
[3]Department of Anatomy and Cell Biology, Yamagata University School of Medicine, Yamagata, Japan
[4]Department of Molecular Genetics, Institute of Biomedical Sciences, Fukushima Medical University School of Medicine, Fukushima, Japan

Keywords: dopamine, green fluorescent protein, Parkinson's disease, striatum, tyrosine hydroxylase

Abstract

The striatum harbors a small number of tyrosine hydroxylase (TH) mRNA-containing GABAergic neurons that express TH immunoreactivity after dopamine depletion, some of which reportedly resembled striatal medium spiny projection neurons (MSNs). To clarify whether the TH mRNA-expressing neurons were a subset of MSNs, we characterized their postnatal development of electrophysiological and morphological properties using a transgenic mouse strain expressing enhanced green fluorescent protein (EGFP) under the control of the rat TH gene promoter. At postnatal day (P)1, EGFP-TH$^+$ neurons were present as clusters in the striatum and, thereafter, gradually scattered ventromedially by P18 without regard to the striatal compartments. They were immunonegative for calbindin, but immunopositive for enkephalin (54.5%) and dynorphin (80.0%). Whole-cell patch-clamp recordings revealed at least two distinct neuronal types, termed EGFP-TH$^+$ Type A and B. Whereas Type B neurons were aspiny and negative for the MSN marker dopamine- and cyclic AMP-regulated phosphoprotein of 32 kDa (DARPP-32), Type A neurons constituted 75% of the EGFP$^+$ cells, had dendritic spines (24.6%), contained DARPP-32 (73.6%) and a proportion acquired TH immunoreactivity after injections of 1-methyl-4-phenyl-1,2,3,6-tetrahydropyridine and 3-nitropropionic acid. The membrane properties and *N*-methyl-D-aspartate : non-*N*-methyl-D-aspartate excitatory postsynaptic current ratio of Type A neurons were very similar to MSNs at P18. However, their resting membrane potentials and spike widths were statistically different from those of MSNs. In addition, the calbindin-like, DARPP-32-like and dynorphin B-like immunoreactivity of Type A neurons developed differently from that of MSNs in the matrix. Thus, Type A neurons closely resemble MSNs, but constitute a cell type distinct from classical MSNs.

Introduction

The striatum is the largest nucleus of the basal ganglia that receives massive dopaminergic inputs from the substantia nigra pars compacta. Although the striatum is essentially dopaminoceptive, it has been repeatedly reported that the striatum itself contains neurons that potentially produce dopamine in humans (Ikemoto *et al.*, 1997; Porritt *et al.*, 2000; Cossette *et al.*, 2005), monkeys (Dubach *et al.*, 1987; Betarbet *et al.*, 1997; Palfi *et al.*, 2002; Tande *et al.*, 2006) and rats (Tashiro *et al.*, 1989a,b; Mura *et al.*, 2000; Lopez-Real *et al.*, 2003; Jollivet *et al.*, 2004). The intrinsic dopaminergic neuron is a new addition to the striatal neuronal population and, in addition, the neuron itself is heterogeneous and contains several distinct subtypes. Birth-dating studies using bromodeoxyuridine (BrdU) after 1-methyl-4-phenyl-1,2,3,6-tetrahydropyridine (MPTP) injection revealed that these tyrosine hydroxylase (TH)-immunoreactive neurons resulted from a phenotypic shift of pre-existing GABAergic interneurons (Betarbet *et al.*, 1997; Mao *et al.*, 2001; Tande *et al.*, 2006). They are immunoreactive to the GABA-synthesizing enzyme glutamic acid decarboxylase (GAD) and are mostly immunonegative for calbindin, a Ca^{2+}-binding protein and a marker for the medium spiny projection neurons (MSNs) in the matrix compartment (Gerfen, 1992). In the mouse striatum, there are few cells, if any, that are immunoreactive for TH, but they do appear after dopamine depletion by a combined treatment of MPTP and 3-nitropropionic acid (3-NPA) (Nakahara *et al.*, 2001) or a 6-hydroxydopamine treatment (Darmopil *et al.*, 2008). These cells contain a small population of aspiny calretinin-positive neurons and a large number of aspiny and spiny neurons that express calbindin as well as enkephalin or dynorphin, markers for

Correspondence: Toshihiko Aosaki, as above.
E-mail: aosaki@tmig.or.jp

**Present address*: Department of Pharmaceutical Sciences, Tokyo Metropolitan Institute of Public Health, Shinjuku, Tokyo 169-0073, Japan.

†Present address: Yamagata Prefectural Kahoku Hospital, Kahoku, Yamagata 999-3511, Japan.

‡Present address: Systems Neuroscience Section, Primate Research Institute, Kyoto University, Inuyama, Aichi 484-8506, Japan.

Received 4 March 2011, revised 3 August 2011, accepted 9 August 2011

indirect or direct pathway MSNs, respectively, suggesting that there might be a population of MSNs that acquire TH immunoreactivity after dopamine depletion in rodents (Darmopil *et al.*, 2008).

In contrast, Ibanez-Sandoval *et al.* (2010) recently reported the first detailed electrophysiological characterization of TH-positive neurons in the adult mouse striatum of a bacterial artificial chromosome transgenic mouse strain that expresses enhanced green fluorescent protein (EGFP). They found at least four electrophysiologically distinct subtypes of EGFP-TH$^+$ neurons, none of which were retrogradely labeled by injection of rhodamine beads into both the globus pallidus and substantia nigra, indicating that they are aspiny TH$^+$/GABAergic interneurons.

These seemingly contradictory results prompted us to characterize the postnatal development of TH mRNA-expressing EGFP$^+$ neurons in transgenic mice harboring a 9-kb TH promoter/EGFP reporter construct, in order to contrast them with MSNs to see whether or not they constitute a distinct subset of MSNs (Sawamoto *et al.*, 2001; Matsushita *et al.*, 2002; Baker *et al.*, 2003). We report here that the most numerous developing EGFP-TH$^+$ neurons were aspiny or spiny GABAergic neurons that were immunoreactive for dynorphin, enkephalin and dopamine- and cyclic AMP-regulated phosphoprotein of 32 kDa (DARPP-32), some of which became electrophysiologically indistinguishable from MSNs late in development. However, their immunohistochemical and electrophysiological properties followed different developmental time courses compared with MSNs and their distribution was not constrained by the striosome-matrix borders, suggesting that they constitute a unique neuronal subtype distinct from classical, direct and indirect pathway MSNs in the striatum.

Materials and methods

Transgenic mice

Production of the TH-EGFP transgenic mice has been described in previous studies (Sawamoto *et al.*, 2001; Matsushita *et al.*, 2002). The transgene construct contained the 9.0-kb 5′-flanking region of the rat TH gene, the second intron of the rabbit β-globin gene, cDNA encoding EGFP (Clontech, Palo Alto, CA, USA) and polyadenylation signals of the rabbit β-globin and Simian virus 40 early genes. In the present study, the TH-EGFP/21–31 strain was used, and the strain was maintained by breeding to C57BL/6J inbred mice. Transgenic mice were identified by polymerase chain reaction amplification of the EGFP sequence from tail DNA. The Animal Care and Use Committee of the Tokyo Metropolitan Institute of Gerontology approved all experimental procedures using laboratory animals.

Immunohistochemistry

The anterior region of the striatum is developmentally distinct from the posterior region (Nery *et al.*, 2002). We examined the anterior part of the striatum in this study. Mice were deeply anesthetized with isoflurane and intracardially perfused with phosphate-buffered saline (PBS) followed by 4% paraformaldehyde solution in PBS. Brains were dissected from the mice and immersed in the same solution at 4 °C overnight. The fixed tissues were cut into sections (50 μm) with a ZERO 1 SuperMicroslicer (Dosaka, Kyoto, Japan). The multiple immunofluorescence technique was used to investigate colocalization of EGFP with other markers. Sections were blocked with 10% normal goat or donkey serum and 0.3% Triton X-100 in PBS for 1 h, and then incubated for 24 h with primary antibodies at 4 °C. Antibodies presented here were as follows: rabbit anti-TH polyclonal antibody (1 : 400; Chemicon, Temecula, CA, USA), rabbit anti-choline acetyltransferase antibody (1 : 400; Chemicon), rabbit anti-calretinin polyclonal antibody (1 : 400; Swant, Bellizona, Switzerland), goat anti-calretinin polyclonal antibody (1 : 2000; Chemicon), rabbit anti-calbindin D-28k monoclonal antibody (1 : 500; Chemicon), rabbit anti-GAD65/67 polyclonal antibody (1 : 500; Sigma-Aldrich, St Louis, MO, USA), rabbit anti-DARPP-32 polyclonal antibody (1 : 100; Chemicon), mouse anti-DARPP-32 antibody (1 : 125; BD Biosciences PharMingen, San Diego, CA, USA), rabbit anti-Met-enkephalin antibody (1 : 250; Biomol, Hamburg, Germany), rabbit anti-dynorphin B antibody (1 : 250; Bachem, Bubendorf, Switzerland), rat anti-green fluorescence protein (GFP) monoclonal antibody (1 : 500; Nacalai Tesque, Kyoto, Japan), mouse anti-Neuronal Nuclei (NeuN) monoclonal antibody (1 : 500; Chemicon), rabbit anti-TuJ1 polyclonal antibody (1 : 2000; Covance, Emeryville, CA, USA) and goat anti-doublecortin polyclonal antibody (1 : 500; Santa Cruz Biotechnology, Santa Cruz, CA, USA). After the sections had been washed with PBS containing 0.1% normal goat or donkey serum, 1% bovine serum albumin and 0.3% Triton X-100, they were incubated with Alexa Fluor 488-, 647- or Cy3-conjugated anti-rabbit, anti-mouse or anti-goat IgG secondary antibody or Cy3-conjugated streptavidin (Molecular Probes, Eugene, OR, USA; Jackson ImmunoResearch Inc., West Grove, PA, USA). The sections were washed with PBS containing 1% normal goat or donkey serum, 1% bovine serum albumin and 0.3% Triton X-100, and mounted in Aquatex (Merck, Darmstadt, Germany). In some experiments, Triton X-100 was omitted because the detergent disturbed GAD immunostaining of somatic profiles (Jinno & Kosaka, 2004). Low-magnification images were acquired using an MVX10 fluorescence microscope (Olympus, Tokyo, Japan) and high-resolution images were taken using an LSM 5 Pascal confocal laser scanning microscope equipped with a high numerical aperture oil-immersion objective lens (63×, NA 1.40, Zeiss, Oberkochen, Germany). Images were acquired as stacked files through the whole section thickness at an optimal step size (1.0 μm). Montages were made from maximum intensity projections of confocal z-stacks of EGFP-positive neurons. The contrast of digital images was enhanced with Adobe Photoshop (Adobe Systems Inc., San Jose, CA, USA).

Quantification of EGFP-positive neurons and EGFP-negative medium-sized neurons expressing calbindin-like, DARPP-32-like and dynorphin B-like immunoreactivity at postnatal day (P)2, P8 and P18–26 was carried out in randomly chosen areas in 2–4 randomly chosen striatal sections from 2 to 3 animals. The data are presented as a percentage of immunopositive or immunonegative cells out of all cells counted. Statistical analysis was performed using a chi-square test from a contingency table of the number of immunopositive and immunonegative cells, with the resultant graph shown in Fig. 4. The threshold for statistical significance was set at $P < 0.05$.

Electrophysiology

Whole brains taken from 2- to 20-day-old EGFP-TH$^+$ transgenic mice under anesthesia were placed in ice-cold artificial cerebraspinal fluid (CSF) containing the following (in mM): 124 NaCl, 3 KCl, 1 NaH_2PO_4, 1.2 $MgCl_2$, 2.4 $CaCl_2$, 10 glucose, buffered to pH 7.4 with $NaHCO_3$ (26 mM) saturated with 95% O_2 and 5% CO_2. Parasagittal or coronal slices (250 μm thick), cut using a Pro 7 Linear Microslicer (Dosaka), were continuously perfused with artificial CSF at a rate of 1–2 mL/min at 30 °C. Whole-cell patch-clamp recordings were collected by an EPC9/2 amplifier (Heka Elektronik, Lambrecht/Pfalz, Germany), with infrared differential contrast and fluorescent visualization using a BX50WI microscope (Olympus) with two charge-coupled device cameras (Hamamatsu Photonics, Shizuoka,